

SUPPLEMENTARY MATERIALS

Rhenium(I) complexes with phenanthrolines bearing electron withdrawing Cl and electron donating CH₃ substituents - synthesis, photophysical, thermal and electrochemical properties with electroluminescence ability

Anna Świtlicka^a, Tomasz Klemens^a, Barbara Machura^a, Ewa Schab-Balcerzak^{a,b}, Katarzyna Laba^{b,c}, Mieczysław Lapkowski^{b,c}, Marzena Grucela^b, Jacek Nycz^a, Marcin Szala^a, Magdalena Kania^d

^aInstitute of Chemistry, University of Silesia, 9 Szkolna Str., 40-006 Katowice, Poland,

^bCentre of Polymer and Carbon Materials, Polish Academy of Sciences, 34 M. Curie-Sklodowska Str., 41-819 Zabrze, Poland

^cSilesian University of Technology, Faculty of Chemistry, 9 Strzody Str., 44-100 Gliwice, Poland

^dMass Spectrometry Group, Institute of Organic Chemistry, Polish Academy of Sciences, Kasprzaka 44/52, PO Box 58, 01-224 Warszawa 42, Poland

Physical measurements: The IR spectra were recorded on a Nicolet iS5 FTIR spectrophotometer in the spectral range 4000–400 cm⁻¹ with the samples in the form of KBr pellets. The electronic spectra were measured on a Perkin Elmer Lambda 40 UV/Vis Spectrometer (in CH₃CN and CHCl₃ solution) and Jasco V570 UV-V-NIR Spectrometer (in solid state as film deposited on glass substrate and as blends with PVK and PVK:PBD mixture on glass substrate). The ¹H NMR and ¹³C NMR spectra were recorded (295 K) on Bruker Avance 400 NMR spectrometer at a resonance frequency of 400 MHz for ¹H NMR spectra and 100 MHz for ¹³C NMR spectra or on Bruker Avance 500 NMR spectrometer at a resonance frequency of 500 MHz for ¹H NMR spectra and 125 MHz for ¹³C NMR spectra using DMSO-d₆ or CDCl₃ as solvent and TMS as an internal solvent.

The HR MS measurements were performed using MALDI Synapt G2-S HDMS (*Waters Inc*) mass spectrometer equipped with an electrospray (ESI) ion source and q-TOF type mass analyzer. The instrument was controlled and recorded data were processed using *MassLynx V4.1* software package (*Waters Inc*). The analyzed samples were dissolved in a mixture of MeOH and CH₂Cl₂ (3/1).

The ESI HR MS spectra were recorded in the positive ion mode, in the *m/z* range 100 – 3000. As a desolvation and a cone gas nitrogen was used. The ion source parameters were optimized for each

analyzed sample to obtain the best intensity of the signals corresponding to the analyzed compound. The source temperature and desolvation temperature was kept at 80 °C and 150 °C, respectively, for all measurements.

Steady-state luminescence spectra of solid state and solution samples were measured on the FLS-980 fluorescence spectrophotometer equipped with a 450 W Xe lamp and high-gain photomultiplier PMT + 500nm (Hamamatsu, R928P) detector. The PL lifetime measurement was performed with a time correlated single photon counting (TCSPC) or multi-channel scaling (MCS) method. Excitation wavelength (375 nm or 470 nm) for TCSPC was obtained using the TCSPC diode with various pulse periods as light source. For MCS excitation wavelength was obtained using 60W microsecond Xe flashlamp. Photoluminescence spectra (PL) in solid state as thin film and as blends with PVK and with PVK:PBD (50:50) mixture deposited on glass substrate were registered using Varian Carry Eclipse Fluorescence Spectrophotometer. Differential Scanning Calorimetry (DSC) was performed with a TA-DSC 2010 apparatus, under nitrogen atmosphere with heating/cooling rate 20 deg/min using sealed aluminum pans. Thermogravimetric analysis (TGA) was done using a Mettler Toledo TGA/DSC STARe system over the temperature range from 25–600°C at a heating rate of 10° C min⁻¹ under a constant nitrogen flow of 60 mL min⁻¹. The obtained TGA data were analyzed using the Mettler-Toledo Star System SW 9.30. Electrochemical measurements were carried out using eDAQ EA161 potentiostat. Cyclic voltammetry experiments were conducted in Ar purged 0.2 M solutions of electrolyte Bu₄NPF₆ (Aldrich, 99%) in acetonitrile (Aldrich, HPLC grade) at room temperature. The electrochemical cell comprised of a 1 mm diameter platinum disc, a platinum coil and a silver coil electrode as a working electrode, a counter electrode and a quasi-reference electrode, respectively. In each electrochemical experiment the reference electrode potential was monitored using ferrocene (Fc) as the internal standard. All electrochemical measurements were performed in 1.0 mM concentrations of the investigated compounds using a scan rate of 100 mV s⁻¹. The approximation of IP-EA energy level values was calculated from the oxidation and reduction potential onsets by assuming the absolute energy level of Fc/Fc⁺ as -5.1 eV to vacuum. The electrochemical band gap was taken as the difference between the electron affinity and ionization potential energy levels. Active layers thickness was measured by atomic force microscopy (AFM) Topometrix Explorer TMX 2000. Current – voltage measurements were carried out using a Keithley 2401 source-measure unit.

Tables:

Table S1. Crystal data and structure refinement of **1**, **3** and **5** complexes.

Table S2. Comparison of experimental and theoretical bond lengths [Å] and angles [°] for **1**, **3** and **5**.

Table S3. Short intra- and intermolecular contacts detected in the structures of the tricarbonyl rhenium(I) complexes.

Table S4. The energies and characters of the selected spin-allowed electronic transitions for **1** calculated with the TDDFT/B3LYP method, together with assignment to the experimental absorption bands.

Table S5. The energies and characters of the selected spin-allowed electronic transitions for **2** calculated with the TDDFT/B3LYP method, together with assignment to the experimental absorption bands.

Table S6. The energies and characters of the selected spin-allowed electronic transitions for **3** calculated with the TDDFT/B3LYP method, together with assignment to the experimental absorption bands.

Table S7. The energies and characters of the selected spin-allowed electronic transitions for **4** calculated with the TDDFT/B3LYP method, together with assignment to the experimental absorption bands.

Table S8. The energies and characters of the selected spin-allowed electronic transitions for **5** calculated with the TDDFT/B3LYP method, together with assignment to the experimental absorption bands.

Table S9. Percentage contributions of Re, CO, phen and Cl units to the selected occupied and unoccupied molecular orbitals of **1** in the ground state, calculated at the DFT/B3LYP/DEF2-TZVPD level.

Table S10. Percentage contributions of Re, CO, phen and Cl units to the selected occupied and unoccupied molecular orbitals of **2** in the ground state, calculated at the DFT/B3LYP/DEF2-TZVPD level.

Table S11. Percentage contributions of Re, CO, phen and Cl units to the selected occupied and unoccupied molecular orbitals of **3** in the ground state, calculated at the DFT/B3LYP/DEF2-TZVPD level.

Table S12. Percentage contributions of Re, CO, phen and Cl units to the selected occupied and unoccupied molecular orbitals of **4** in the ground state, calculated at the DFT/B3LYP/DEF2-TZVPD level.

Table S13. Percentage contributions of Re, CO, phen and Cl units to the selected occupied and unoccupied molecular orbitals of **5** in the ground state, calculated at the DFT/B3LYP/DEF2-TZVPD level.

Table S14. Percentage contributions of Re, CO, phen and Cl units to the the HSOMO and LSOMO involved in TD-DFT triplet excitations

Figures:

Figure S1. A view of the crystal packing showing intermolecular $\pi-\pi$ stacking interactions for **1**, **3** and **5**

Figure S2. Excitation and emission spectra together with PL lifetime curves for **1-5**.

Figure S3. Emission spectra of PVK and PVK:PBD 1:1 films on glass.

Figure S4. Frontier molecular orbitals of **1-5** computed at the DFT/B3LYP/DEF2-TZVPD level .

Figure S5. Isodensity surface electron spin density for compounds **1-5** at its T_1 state geometry calculated at DFT/UB3LYP/def2-TZVPD level of theory associated with the PCM model in CH_3CN as a solvent.

Figure S6. ^1H NMR spectrum of **1**

Figure S7. ^1H NMR spectrum of **2**

Figure S8. ^1H NMR spectrum of **3**

Figure S9. ^1H NMR spectrum of **4**

Figure S10. ^1H NMR spectrum of **5**

Figure S11. ^{13}C NMR spectrum of **1**

Figure S12. ^{13}C NMR spectrum of **2**

Figure S13. ^{13}C NMR spectrum of **3**

Figure S14. ^{13}C NMR spectrum of **4**

Figure S15. ^{13}C NMR spectrum of **5**

Figure S16. DSC thermograms (heating 20 deg/min) of all investigated complexes: (a) compound **1**, (b) **2**, (c) **3**, (d) **4** and (e) **5**.

Table S1. Crystal data and structure refinement of **1**, **3** and **5** complexes.

	1	3	5
Empirical formula	C ₁₈ H ₁₂ Cl ₃ N ₂ O ₃ Re	C ₁₅ H ₅ Cl ₄ N ₂ O ₃ Re	C ₁₇ H ₁₀ Cl ₂ N ₃ O ₃ Re
Formula weight	596.86	589.22	561.39
Temperature [K]	298.0(2)	298.0(2)	298.0(2)
Wavelength [Å]	0.71073	0.71073	0.71073
Crystal system	monoclinic	monoclinic	triclinic
Space group	P2 ₁ /n	P2 ₁ /c	P-1
Unit cell dimensions [Å, °]	10.8752(5) 32.4799(13) 10.9891(4) 98.199(3)	a = 6.6848(5) b = 20.9252(16) c = 12.6551(7) β = 100.710(7)	a = 8.3105(3) b = 9.7851(4) c = 12.3202(5) α = 84.319(3) β = 85.261(3) γ = 67.529(4)
Volume [Å ³]	3842.0(3)	1739.4(2)	920.16(7)
Z	8	4	2
Density (calculated) [Mg/m ³]	2.064	2.250	2.026
Absorption coefficient [mm ⁻¹]	6.764	7.618	6.915
F(000)	2272	1104	532
Crystal size [mm]	0.24 x 0.11 x 0.04	0.19 x 0.09 x 0.03	0.09 x 0.09 x 0.04
θ range for data collection [°]	3.41 to 25.05	3.35 to 25.05	3.88 to 25.05
Index ranges	-11 ≤ h ≤ 12 -38 ≤ k ≤ 33 -13 ≤ l ≤ 12	-7 ≤ h ≤ 7 -24 ≤ k ≤ 24 -15 ≤ l ≤ 15	-9 ≤ h ≤ 9 -11 ≤ k ≤ 11 -13 ≤ l ≤ 14
Reflections collected	28790	8748	7649
Independent reflections	6774 (R _{int} = 0.063)	3069 (R _{int} = 0.045)	3248 (R _{int} = 0.048)
Completeness to 2θ=50° [%]	99.7	99.8	99.8
Max. and min. transmission	1.000 and 0.483		1.000 and 0.362
Data / restraints / parameters	6774 / 0 / 493	3069 / 0 / 236	3248 / 0 / 236
Goodness-of-fit on F ²	0.969	1.233	0.971
Final R indices [I>2σ(I)]	R ₁ = 0.0494 wR ₂ = 0.0965	R ₁ = 0.0566 wR ₂ = 0.1067	R ₁ = 0.0298 wR ₂ = 0.0484
R indices (all data)	R ₁ = 0.0631 wR ₂ = 0.1008	R ₁ = 0.0801 wR ₂ = 0.1122	R ₁ = 0.0404 wR ₂ = 0.0512
Largest diff. peak and hole[eÅ ⁻³]	3.08 and -2.55	1.41 and -2.75	0.76 and -1.00
CCDC number	1501825	1501826	1501827

Table S2. Experimental and theoretical bond lengths [Å] and angles [°] for **1**, **3** and **5**.

Bond lengths	Exp.	Opt.	Bond angles	Exp.	Opt.
		S ₀			S ₀
1					
Re(1)–C(1)	1.909(11)	1.92942	C(2)–Re(1)–C(1)	83.8(5)	83.798
Re(1)–C(2)	1.881(11)	1.92776	C(3)–Re(1)–C(1)	90.2(5)	90.955
Re(1)–C(3)	1.903(11)	1.91518	C(3)–Re(1)–C(2)	91.2(4)	90.903
Re(1)–N(1)	2.184(7)	2.23886	C(1)–Re(1)–N(1)	171.0(4)	172.511
Re(1)–N(2)	2.211(7)	2.25072	C(2)–Re(1)–N(1)	100.1(4)	100.873
Re(1)–Cl(1)	2.484(2)	2.54663	C(3)–Re(1)–N(1)	97.8(4)	94.795
C(1)–O(1)	1.141(13)	1.16517	C(1)–Re(1)–N(2)	100.6(4)	100.954
C(2)–O(2)	1.179(12)	1.16523	C(2)–Re(1)–N(2)	172.1(4)	172.362
C(3)–O(3)	1.139(12)	1.91518	C(3)–Re(1)–N(2)	95.3(3)	94.965
			N(1)–Re(1)–N(2)	74.7(3)	73.802
			C(1)–Re(1)–Cl(1)	90.3(4)	90.499
			C(2)–Re(1)–Cl(1)	88.8(3)	90.606
			C(3)–Re(1)–Cl(1)	179.6(3)	178.010
			N(1)–Re(1)–Cl(1)	81.73(19)	83.644
			N(2)–Re(1)–Cl(1)	84.73(19)	83.422
Re(2)–C(19)	1.917(12)		C(19)–Re(2)–C(20)	82.4(5)	
Re(2)–C(20)	1.921(11)		C(19)–Re(2)–C(21)	89.3(5)	
Re(2)–C(21)	1.938(12)		C(20)–Re(2)–C(21)	90.4(5)	
Re(2)–N(3)	2.213(7)		C(19)–Re(2)–N(3)	172.8(4)	
Re(2)–N(4)	2.192(8)		C(20)–Re(2)–N(3)	100.3(4)	
Re(2)–Cl(2)	2.485(2)		C(21)–Re(2)–N(3)	97.3(4)	
C(19)–O(4)	1.136(13)		C(19)–Re(2)–N(4)	102.4(4)	
C(20)–O(5)	1.126(12)		C(20)–Re(2)–N(4)	174.2(4)	
C(21)–O(6)	1.085(12)		C(21)–Re(2)–N(4)	93.0(4)	
			N(3)–Re(2)–N(4)	74.6(3)	
			C(19)–Re(2)–Cl(4)	91.1(3)	
			C(20)–Re(2)–Cl(4)	93.4(3)	
			C(21)–Re(2)–Cl(4)	176.2(3)	
			N(3)–Re(2)–Cl(4)	82.09(19)	
			N(4)–Re(2)–Cl(4)	83.2(2)	
3					
Re(1)–C(1)	1.914(15)	1.93260	C(2)–Re(1)–C(1)	88.5(6)	88.627
Re(1)–C(2)	1.895(16)	1.93445	C(3)–Re(1)–C(1)	90.5(6)	90.187
Re(1)–C(3)	1.919(17)	1.91850	C(3)–Re(1)–C(2)	90.9(7)	90.208
Re(1)–N(1)	2.155(9)	2.21727	C(1)–Re(1)–N(1)	173.4(5)	171.907
Re(1)–N(2)	2.173(10)	2.20584	C(2)–Re(1)–N(1)	97.7(5)	98.658
Re(1)–Cl(1)	2.462(4)	2.53286	C(3)–Re(1)–N(1)	91.4(5)	93.289
C(1)–O(1)	1.145(15)	1.16438	C(1)–Re(1)–N(2)	99.2(5)	98.734
C(2)–O(2)	1.147(17)	1.16428	C(2)–Re(1)–N(2)	171.4(6)	171.791
C(3)–O(3)	1.091(17)	1.16846	C(3)–Re(1)–N(2)	92.7(5)	93.378
			N(1)–Re(1)–N(2)	74.4(4)	73.782
			C(1)–Re(1)–Cl(1)	94.3(4)	92.339
			C(2)–Re(1)–Cl(1)	93.3(5)	92.182
			C(3)–Re(1)–Cl(1)	173.6(5)	176.563
			N(1)–Re(1)–Cl(1)	83.3(3)	83.911
			N(2)–Re(1)–Cl(1)	82.5(3)	83.936
5					
Re(1)–C(1)	1.884(7)	1.93143	C(2)–Re(1)–C(1)	87.1(2)	88.875
Re(1)–C(2)	1.919(5)	1.93227	C(3)–Re(1)–C(1)	89.2(3)	90.155
Re(1)–C(3)	1.895(6)	1.91613	C(3)–Re(1)–C(2)	89.7(2)	90.133
Re(1)–N(1)	2.158(4)	2.22112	C(1)–Re(1)–N(1)	173.1(2)	172.265
Re(1)–N(2)	2.191(4)	2.21680	C(2)–Re(1)–N(1)	97.22(19)	98.041
Re(1)–Cl(1)	2.4848(13)	2.54290	C(3)–Re(1)–N(1)	96.2(2)	93.274
C(1)–O(1)	1.165(7)	1.16537	C(1)–Re(1)–N(2)	100.2(2)	98.074
C(2)–O(2)	1.144(6)	1.16535	C(2)–Re(1)–N(2)	172.3(2)	172.254
C(3)–O(3)	1.160(6)	1.16889	C(3)–Re(1)–N(2)	92.79(18)	93.251
			N(1)–Re(1)–N(2)	75.28(14)	74.824
			C(1)–Re(1)–Cl(1)	92.07(19)	92.197
			C(2)–Re(1)–Cl(1)	92.83(16)	92.195
			C(3)–Re(1)–Cl(1)	177.26(16)	176.722
			N(1)–Re(1)–Cl(1)	82.37(10)	84.117
			N(2)–Re(1)–Cl(1)	84.58(10)	84.160

Table S3. Short intra- and intermolecular contacts detected in the structures of the rhenium(I) complexes.

D—H…A	D—H	H…A	D…A [Å]	D—H…A [°]
1				
C(8)—H(8)…Cl(2)	0.93	2.72	3.108(10)	106.00
C(16)—H(16B)…Cl(3)	0.96	2.58	2.944(17)	103.00
C(23)—H(23)…Cl(1)#1	0.93	2.74	3.643(10)	163.00
C(27)—H(27)…Cl(5)	0.96	2.69	3.078(11)	106.00
3				
C(8)—H(8)…Cl(2)	0.93	2.74	3.095(14)	104.00
5				
C(4)—H(4)…N(3)#2	0.93	2.59	3.425(8)	149.00
C(6)—H(6)…Cl(2)	0.93	2.71	3.073(6)	104.00
C(12)—H(12)…Cl(1)#3	0.93	2.81	3.664(5)	154.00
C(16)—H(16C)…O(2)#4	0.96	2.46	3.269(10)	141.00

Symmetry codes: #1: 1/2-x, -1/2+y, 1/2-z; #2: -1+x, y, z; #3: 1+x, y, z; #4: 1-x, 2-y, 1-z;

Table S4. The energies and characters of the selected spin-allowed electronic transitions for **1** calculated with the TDDFT/B3LYP method, together with assignment to the experimental absorption bands.

Experimental absorption λ; nm (10 ⁻³ ε; M ⁻¹ cm ⁻¹)	Calculated transitions				
	Major contribution (%)	Character	E [eV]	λ [nm]	Oscillator strength
386.10 (6.08)	H—1 → L (95%)	MLLCT	3.02	409.33	0.0959
	H → L+1 (81%)	MLLCT	3.37	366.92	0.0433
	H—1 → L+1 (94%)	MLLCT	3.44	359.75	0.0624
333.09 (9.12)	H—2 → L+1 (97%)	MLLCT	3.79	326.93	0.0159
284.99 (28.58)	H—4 → L (47%)	IL/LLCT	4.26	290.93	0.1907
	H—4 → L+1 (38%)	IL/LLCT	4.51	274.62	0.1161
	H—6 → L (33%)	LLCT/LMCT	4.55	272.05	0.2572
	H → L+4 (26%)	MLLCT/d-d			
215.91 (55.60)	H—5 → L+1 (73%)	LLCT/IL	4.80	258.17	0.1047
	H—4 → L+2 (61%)	IL/LLCT	5.61	220.99	0.2970
	H—3 → L+4 (5%)	IL/LLCT/d-d	5.68	218.05	0.1503

Table S5. The energies and characters of the selected spin-allowed electronic transitions for **2** calculated with the TDDFT/B3LYP method, together with assignment to the experimental absorption bands.

Experimental absorption λ ; nm ($10^{-3} \epsilon$; M ⁻¹ cm ⁻¹)	Calculated transitions				
	Major contribution (%)	Character	E [eV]	λ [nm]	Oscillator strength
380.57 (5.61)	H-1 → L (94%)	MLLCT	3.04	406.84	0.0804
	H → L+1 (82%)	MLLCT	3.29	376.58	0.0270
	H-1 → L+1 (96%)	MLLCT	3.39	364.76	0.0494
327.46 (7.19)	H-2 → L+1 (98%)	MLLCT	3.75	330.79	0.0094
270.70 (38.85)	H-4 → L (38%)	IL/LLCT	4.30	288.11	0.1695
	H-4 → L+1 (57%)	IL/LLCT	4.52	274.01	0.1634
	H → L+4 (32%)	MLLCT/d-d	4.58	270.45	0.3279
	H-2 → L+3 (45%)	MLLCT/d-d	4.78	259.30	0.1465
231.38 (42.38)	H-8 → L+1 (36%)	IL	5.34	232.04	0.1470
	H → L+6 (23%)	MLLCT	5.41	229.11	0.0622
	H-1 → L+9 (21%)	MLLCT/d-d			
215.64 (66.61)	H-4 → L+2 (52%)	IL/LLCT	5.64	219.60	0.2882
	H-2 → L+6 (35%)	MLLCT	5.77	214.59	0.0610
	H-3 → L+4 (33%)	LLCT/IL/MLCT	5.81	213.32	0.2725
	H-6 → L+2 (25%)	IL/LLCT	5.86	211.30	0.1422
196.12 (53.78)	H-4 → L+4 (66%)	IL/LLCT/LMCT	5.93	208.77	0.0800
	H-5 → L+4 (60%)	LLCT/IL/MLCT	6.1418	201.87	0.0706
	H-6 → L+5 (88%)	LLCT/IL	6.5071	190.54	0.1067

Table S6. The energies and characters of the selected spin-allowed electronic transitions for **3** calculated with the TDDFT/B3LYP method, together with assignment to the experimental absorption bands

Experimental absorption λ ; nm ($10^{-3} \epsilon$; M ⁻¹ cm ⁻¹)	Calculated transitions				
	Major contribution (%)	Character	E [eV]	λ [nm]	Oscillator strength
393.12 (8.85)	H-1 → L (82%)	MLLCT	2.86	432.95	0.0672
	H → L+1 (83%)	MLLCT	2.97	417.29	0.0566
	H-1 → L+1 (97%)	MLLCT	3.04	406.60	0.0311
313.69 (12.50)	H-2 → L (92%)	MLLCT	3.60	343.58	0.0304
	H-2 → L+1 (88%)	MLLCT	3.84	322.78	0.1619
274.97 (43.77)	H-4 → L+1 (93%)	IL/LLCT	4.36	284.16	0.0916
	H-6 → L (57%)	IL/LLCT	4.62	268.36	0.3063
	H-1 → L+3 (44%)	MLLCT/d-d	4.74	261.39	0.1484
	H-2 → L+2 (43%)	MLCT/LLCT	5.08	243.64	0.1499
229.13 (46.99)	H-2 → L+4 (29%)	MLLCT/d-d	5.51	224.72	0.0666
	H-4 → L+2 (50%)	IL/LLCT	5.59	221.65	0.0995
	H-2 → L+4 (70%)	MLLCT/d-d	5.62	220.54	0.1187
214.86 (64.10)	H-4 → L+2 (20%)	IL/LLCT	5.66	218.83	0.1252
	H-5 → L+2 (77%)	LLCT/IL/MLCT	5.69	217.72	0.1230
	H-2 → L+5 (38%)	MLLCT	5.85	211.81	0.1085
197.45 (55.47)	H-6 → L+2 (49%)	IL/LLCT	5.99	206.96	0.2085
	H-4 → L+5 (43%)	IL/LLCT	6.36	194.75	0.0774

Table S7. The energies and characters of the selected spin-allowed electronic transitions for **4** calculated with the TDDFT/B3LYP method, together with assignment to the experimental absorption bands

Experimental absorption λ ; nm ($10^{-3} \epsilon$; M $^{-1}$ cm $^{-1}$)	Calculated transitions				
	Major contribution (%)	Character	E [eV]	λ [nm]	Oscillator strength
384.37 (6.03)	H-1 → L (92%)	MLLCT	2.95	419.32	0.0787
	H → L+1 (92%)	MLLCT	3.11	397.61	0.0420
	H-1 → L+1 (98%)	MLLCT	3.19	387.86	0.0299
268.33 (47.29)	H-3 → L+1 (79%)	IL/LLCT	4.04	306.49	0.0842
	H-1 → L+2 (78%)	MLLCT	4.34	285.59	0.0660
	H-4 → L+1 (77%)	IL/LLCT	4.50	275.48	0.0923
	H-6 → L (41%)	LLCT/IL	4.65	266.53	0.3532
	H-2 → L+3 (41%)	MLLCT/d-d	4.76	260.27	0.2549
212.80 (63.24)	H-8 → L+2 (48%)	IL	5.2545	235.96	0.0726
	H-4 → L+3 (36%)	IL/LLCT	5.7311	216.33	0.1824
	H-1 → L+8 (36%)	MLLCT	5.8706	211.20	0.0941
	H-2 → L+10 (22%)	MLLCT/d-d	5.9256	209.24	0.0686

Table S8. The energies and characters of the selected spin-allowed electronic transitions for **5** calculated with the TDDFT/B3LYP method, together with assignment to the experimental absorption bands

Experimental absorption λ ; nm ($10^{-3} \epsilon$; M $^{-1}$ cm $^{-1}$)	Calculated transitions				
	Major contribution (%)	Character	E [eV]	λ [nm]	Oscillator strength
378.85 (6.04)	H-1 → L (93%)	MLLCT	3.07	403.30	0.0711
	H → L+1 (92%)	MLLCT	3.24	382.13	0.0309
	H-1 → L+1 (97%)	MLLCT	3.33	372.37	0.0176
290.45 (19.72)	H-3 → L+1 (71%)	IL	4.0512	306.05	0.0432
	H-4 → L (42%)	IL/LLCT	4.3860	282.68	0.0752
269.40 (40.40)	H-4 → L+1 (67%)	IL/LLCT	4.5434	272.89	0.1141
	H-6 → L (22%)	LLCT/IL	4.6518	266.53	0.2277
	H-6 → L+1 (30%)	LLCT/IL	4.7992	258.34	0.2094
218.00 (60.20)	H-3 → L+2 (78%)	IL/LLCT	5.3865	230.18	0.1776
	H-3 → L+4 (86%)	IL/LMCT/LLCT	5.6021	221.32	0.0665
	H-8 → L (31%)	IL	5.6588	219.10	0.0791
200.32 (63.46)	H-1 → L+11 (21%)	MLLCT	5.9825	207.24	0.1108
	H-8 → L+1 (25%)	IL	5.9980	206.71	0.0817
	H-9 → L+1 (22%)	IL	6.0802	203.91	0.1530
	H-6 → L+4 (16%)	LLCT/LMCT/IL	6.2380	198.76	0.0788

Table S9. Percentage contributions of Re, CO, phen and Cl units to the selected occupied and unoccupied molecular orbitals of **1** in the ground state, calculated at the DFT/B3LYP/DEF2-TZVPD level.

Orbital	Energy [eV]	Contribution (%)				Character
		Re	3CO	Cl	phen	
LUMO+4	-0.93	20.76	41.12	6.85	31.27	$\pi^*(\text{CO}) + \pi^*(\text{phen}) + d(\text{Re})$
LUMO+3	-1.07	29.09	34.94	0.99	34.98	$\pi^*(\text{phen}) + \pi^*(\text{CO}) + d(\text{Re})$
LUMO+2	-1.34	9.74	14.01	5.86	70.39	$\pi^*(\text{phen}) + \pi^*(\text{CO})$
LUMO+1	-2.37	0.31	0.63	0.07	98.99	$\pi^*(\text{phen})$
LUMO	-2.72	9.11	4.16	2.68	84.05	$\pi^*(\text{phen})$
HOMO	-6.37	43.85	26.55	23.86	5.74	$d(\text{Re}) + \pi(\text{CO}) + \pi(\text{Cl})$
HOMO-1	-6.40	34.93	18.96	17.11	29.00	$d(\text{Re}) + \pi(\text{CO}) + \pi(\text{Cl}) + \pi(\text{phen})$
HOMO-2	-6.82	45.94	27.86	9.14	17.06	$d(\text{Re}) + \pi(\text{CO}) + \pi(\text{phen})$
HOMO-3	-7.07	21.07	11.59	4.22	63.12	$\pi(\text{phen}) + d(\text{Re}) + \pi(\text{CO})$
HOMO-4	-7.46	0.39	0.33	13.81	85.47	$\pi(\text{phen}) + \pi(\text{Cl})$
HOMO-5	-7.83	9.62	5.83	64.45	20.10	$\pi(\text{Cl}) + \pi(\text{phen})$

Table S10. Percentage contributions of Re, CO, phen and Cl units to the selected occupied and unoccupied molecular orbitals of **2** in the ground state, calculated at the DFT/B3LYP/DEF2-TZVPD level.

Orbital	Energy [eV]	Contribution (%)				Character
		Re	3CO	Cl	phen	
LUMO+4	-0.93	19.22	41.16	6.49	33.13	$\pi^*(\text{CO}) + \pi^*(\text{phen}) + d(\text{Re})$
LUMO+3	-1.08	29.54	36.21	1.04	33.21	$\pi^*(\text{CO}) + \pi^*(\text{phen}) + d(\text{Re})$
LUMO+2	-1.34	9.72	15.47	6.32	68.49	$\pi^*(\text{phen}) + \pi^*(\text{CO})$
LUMO+1	-2.45	0.29	0.56	0.06	99.09	$\pi^*(\text{phen})$
LUMO	-2.74	9.05	4.03	2.69	84.23	$\pi^*(\text{phen})$
HOMO	-6.38	43.65	26.69	24.28	5.38	$d(\text{Re}) + \pi(\text{CO}) + \pi(\text{Cl})$
HOMO-1	-6.44	38.24	20.93	19.95	20.88	$d(\text{Re}) + \pi(\text{CO}) + \pi(\text{Cl}) + \pi(\text{phen})$
HOMO-2	-6.85	51.80	31.27	5.96	10.97	$d(\text{Re}) + \pi(\text{CO})$
HOMO-3	-7.23	12.26	6.43	6.94	74.37	$\pi(\text{phen}) + d(\text{Re})$
HOMO-4	-7.51	0.26	0.28	15.11	84.35	$\pi(\text{phen}) + \pi(\text{Cl})$
HOMO-5	-7.86	10.62	6.30	63.63	19.45	$\pi(\text{Cl}) + \pi(\text{phen}) + d(\text{Re})$

Table S11. Percentage contributions of Re, CO, phen and Cl units to the selected occupied and unoccupied molecular orbitals of **3** in the ground state, calculated at the DFT/B3LYP/DEF2-TZVPD level.

Orbital	Energy [eV]	Contribution (%)				Character
		Re	3CO	Cl	phen	
LUMO+4	-1.00	31.98	41.98	10.56	15.48	$\pi^*(\text{CO}) + d(\text{Re}) + \pi^*(\text{phen})$
LUMO+3	-1.22	24.13	43.73	1.15	30.99	$\pi^*(\text{CO}) + \pi^*(\text{phen}) + d(\text{Re})$
LUMO+2	-1.55	8.67	4.76	2.97	83.60	$\pi^*(\text{phen})$
LUMO+1	-2.82	0.31	0.46	0.22	99.01	$\pi^*(\text{phen})$
LUMO	-2.94	7.59	3.66	2.74	86.01	$\pi^*(\text{phen})$
HOMO	-6.41	42.33	27.47	25.47	4.73	$d(\text{Re}) + \pi(\text{CO}) + \pi(\text{Cl})$
HOMO-1	-6.47	40.63	22.67	23.11	13.59	$d(\text{Re}) + \pi(\text{CO}) + \pi(\text{Cl}) + \pi(\text{phen})$
HOMO-2	-6.92	59.64	34.18	0.52	5.66	$d(\text{Re}) + \pi(\text{CO})$
HOMO-3	-7.18	3.97	1.34	9.72	84.97	$\pi(\text{phen})$
HOMO-4	-7.77	2.52	1.80	39.97	55.71	$\pi(\text{phen}) + \pi(\text{Cl})$
HOMO-5	-7.94	10.80	5.62	64.00	19.58	$\pi(\text{Cl}) + \pi(\text{phen}) + d(\text{Re})$

Table S12. Percentage contributions of Re, CO, phen and Cl units to the selected occupied and unoccupied molecular orbitals of **4** in the ground state, calculated at the DFT/B3LYP/DEF2-TZVPD level.

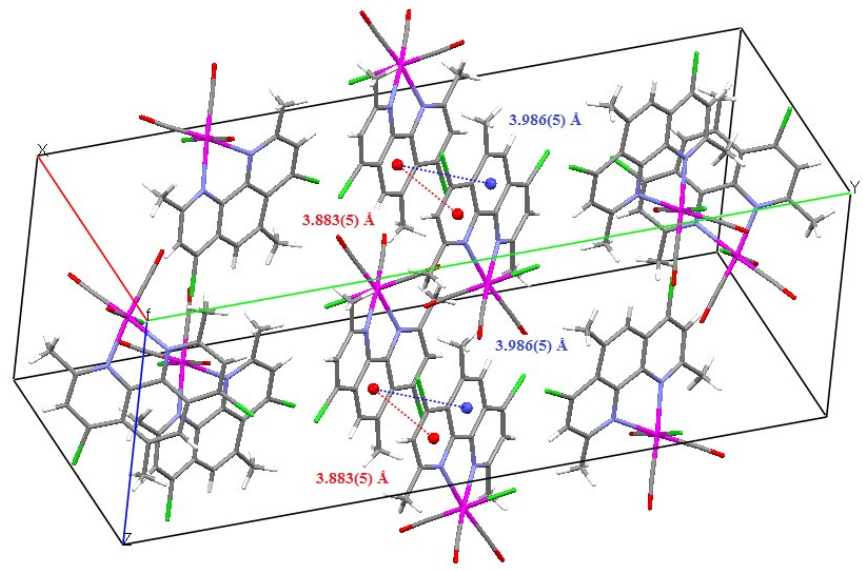
Orbital	Energy [eV]	Contribution (%)				Character
		Re	3CO	Cl	phen	
LUMO+4	-0.97	30.89	39.60	9.78	19.76	$\pi^*(\text{CO}) + \text{d}(\text{Re}) + \pi^*(\text{phen})$
LUMO+3	-1.20	23.87	46.77	1.15	28.21	$\pi^*(\text{CO}) + \pi^*(\text{phen}) + \text{d}(\text{Re})$
LUMO+2	-1.40	8.88	7.79	3.62	79.71	$\pi^*(\text{phen})$
LUMO+1	-2.65	0.30	0.56	0.24	98.90	$\pi^*(\text{phen})$
LUMO	-2.83	7.59	3.75	2.78	85.88	$\pi^*(\text{phen})$
HOMO	-6.40	42.30	27.57	25.15	4.98	$\text{d}(\text{Re}) + \pi(\text{CO}) + \pi(\text{Cl})$
HOMO-1	-6.45	41.34	23.22	23.15	12.29	$\text{d}(\text{Re}) + \pi(\text{CO}) + \pi(\text{Cl}) + \pi(\text{phen})$
HOMO-2	-6.90	59.74	34.23	0.52	5.51	$\text{d}(\text{Re}) + \pi(\text{CO})$
HOMO-3	-7.27	4.28	1.40	14.34	79.98	$\pi(\text{phen}) + \pi(\text{Cl})$
HOMO-4	-7.70	1.64	1.28	33.13	63.95	$\pi(\text{phen}) + \pi(\text{Cl})$
HOMO-5	-7.94	11.82	6.42	64.39	17.37	$\pi(\text{Cl}) + \pi(\text{phen}) + \text{d}(\text{Re})$

Table S13. Percentage contributions of Re, CO, phen and Cl units to the selected occupied and unoccupied molecular orbitals of **5** in the ground state, calculated at the DFT/B3LYP/DEF2-TZVPD level.

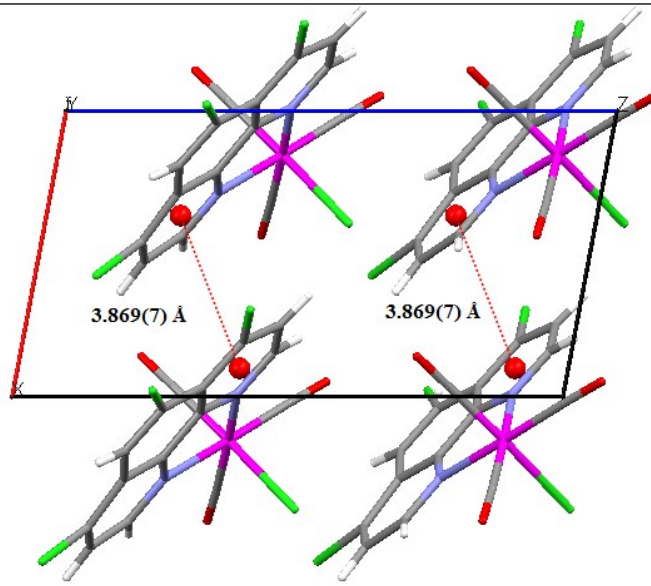
Orbital	Energy [eV]	Contribution (%)				Character
		Re	3CO	Cl	phen	
LUMO+11	-0.05	11.75	29.36	2.09	56.80	$\pi^*(\text{phen}) + \pi^*(\text{CO}) + \text{d}(\text{Re})$
LUMO+5	-0.51	0.70	14.58	0.09	84.63	$\pi^*(\text{phen}) + \pi^*(\text{CO})$
LUMO+4	-0.93	29.49	37.14	9.24	24.13	$\pi^*(\text{CO}) + \text{d}(\text{Re}) + \pi^*(\text{phen})$
LUMO+3	-1.16	25.71	45.81	1.11	27.37	$\pi^*(\text{CO}) + \pi^*(\text{phen}) + \text{d}(\text{Re})$
LUMO+2	-1.28	9.67	11.10	4.48	74.75	$\pi^*(\text{phen}) + \pi^*(\text{CO})$
LUMO+1	-2.49	0.47	0.64	0.32	98.57	$\pi^*(\text{phen})$
LUMO	-2.68	8.29	4.21	3.10	84.40	$\pi^*(\text{phen})$
HOMO	-6.37	42.56	27.88	25.19	4.37	$\text{d}(\text{Re}) + \pi(\text{CO}) + \pi(\text{Cl})$
HOMO-1	-6.44	41.81	23.70	23.89	10.60	$\text{d}(\text{Re}) + \pi(\text{CO}) + \pi(\text{Cl}) + \pi(\text{phen})$
HOMO-2	-6.87	59.67	34.42	0.58	5.33	$\text{d}(\text{Re}) + \pi(\text{CO})$
HOMO-3	-7.13	3.51	1.25	7.27	87.97	$\pi(\text{phen})$
HOMO-4	-7.60	0.50	0.40	14.78	84.32	$\pi(\text{phen}) + \pi(\text{Cl})$
HOMO-5	-7.88	10.13	5.66	69.37	14.84	$\pi(\text{Cl}) + \pi(\text{phen}) + \text{d}(\text{Re})$
HOMO-6	-7.91	9.92	65.10	5.97	19.01	$\pi(\text{CO}) + \pi(\text{phen})$
HOMO-8	-9.08	1.46	1.29	1.79	95.46	$\pi(\text{phen})$
HOMO-9	-9.18	2.68	1.32	4.12	91.88	$\pi(\text{phen})$

Table S14. Percentage contributions of Re, CO, phen and Cl units to the HSOMO and LSOMO involved in TD-DFT triplet excitations

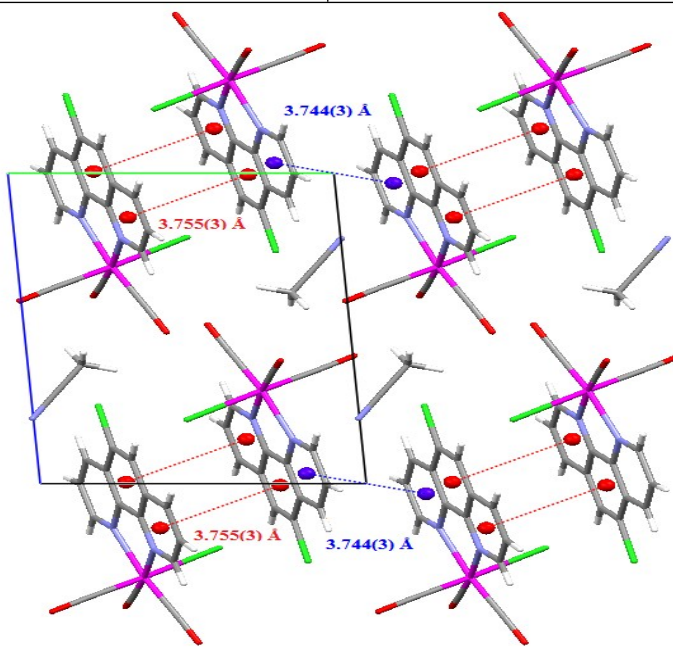
Związek	Orbital	Re	CO	Cl	phen
1	HOMO	36.27	19.37	14.55	29.81
	LUMO	6.64	4.57	1.74	87.05
2	HOMO	43.51	23.41	20.16	12.92
	LUMO	4.20	4.79	2.13	88.88
3	HOMO	40.91	22.36	20.99	15.74
	LUMO	7.58	4.81	2.23	85.38
4	HOMO	41.18	22.61	20.86	15.35
	LUMO	8.13	5.00	2.38	84.49
5	HOMO	42.16	23.45	21.05	13.34
	LUMO	8.95	5.51	2.72	82.82



1



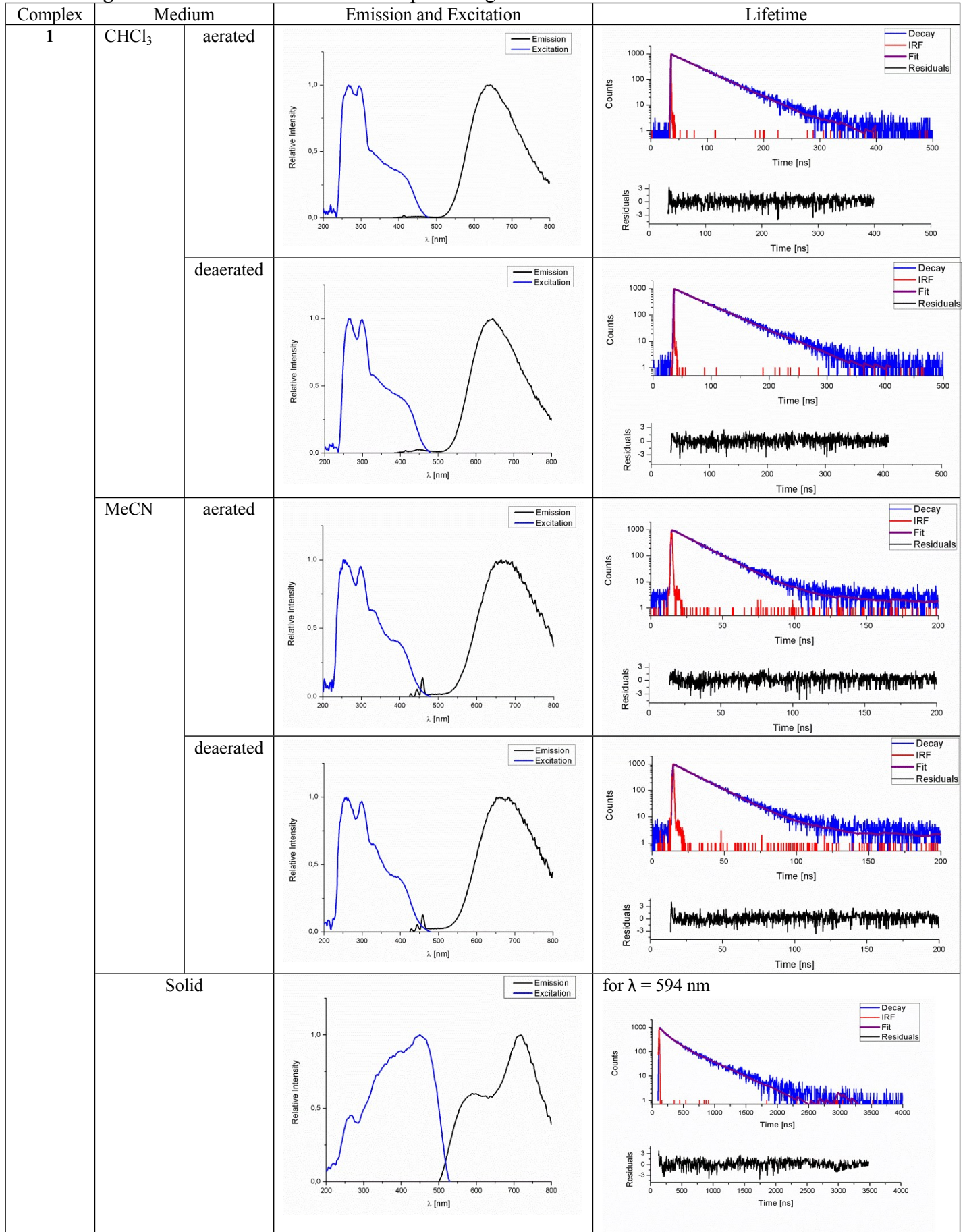
3

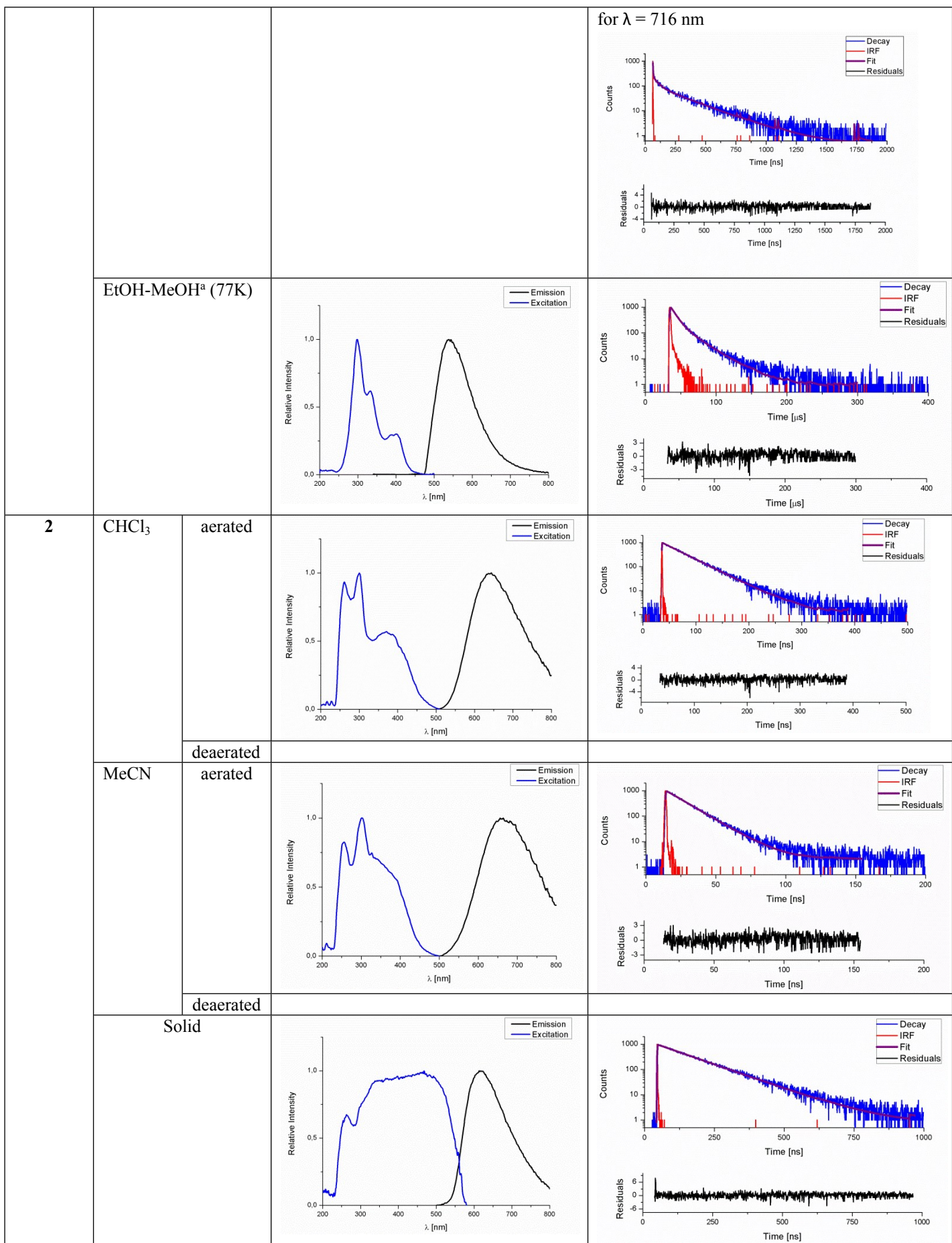


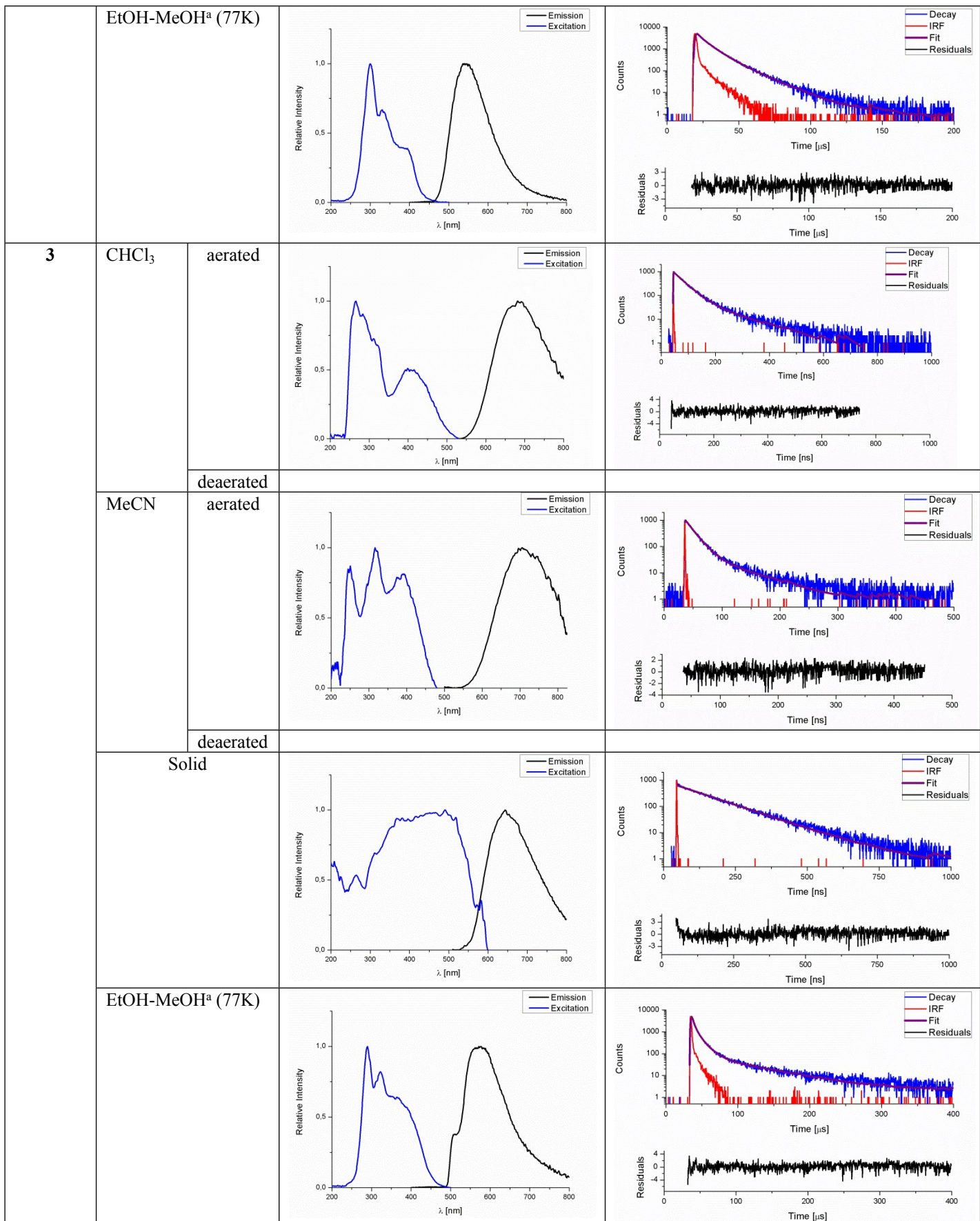
5

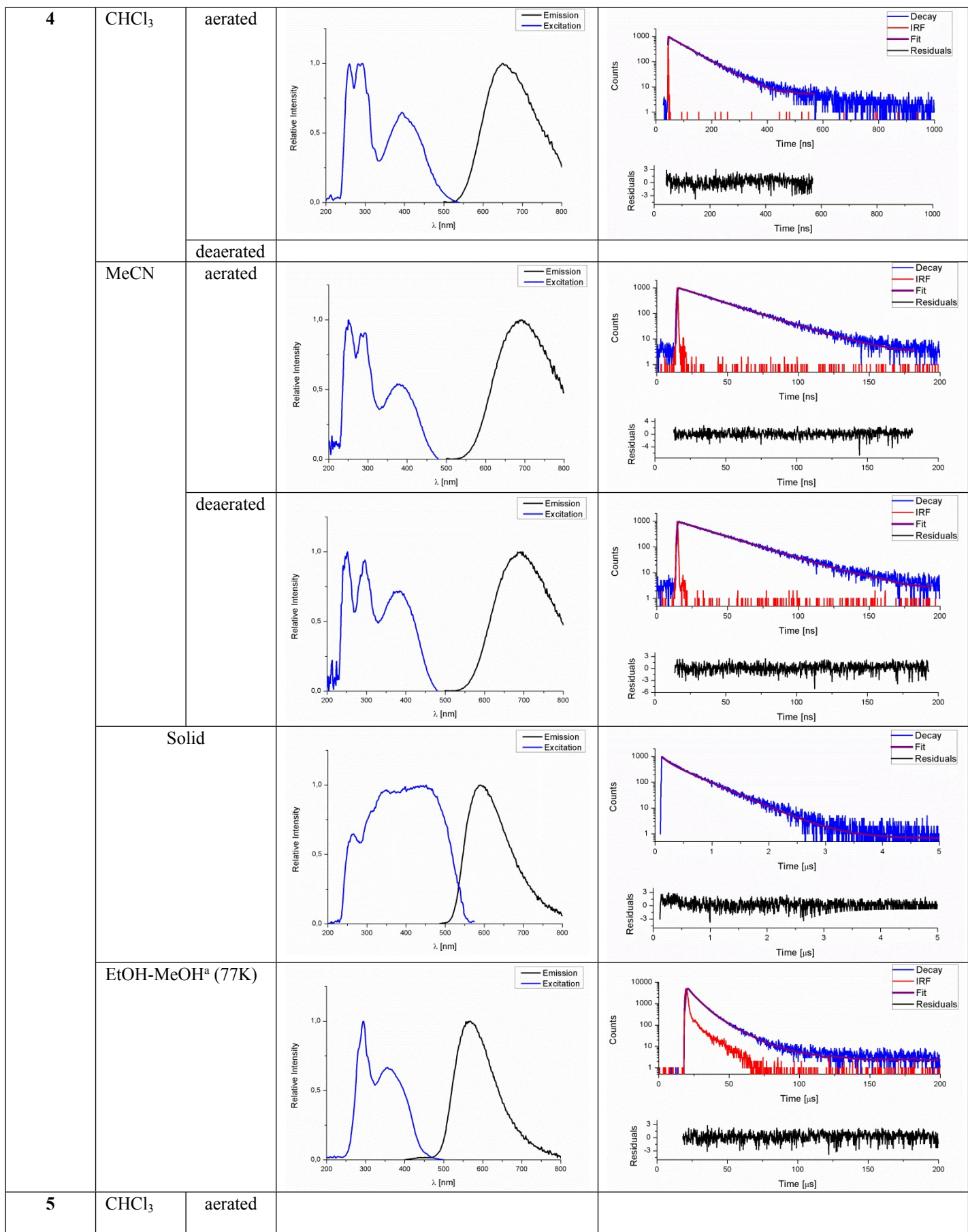
Figure S1. A view of the crystal packing showing intermolecular $\pi\cdots\pi$ stacking interactions for **1**, **3** and **5**.

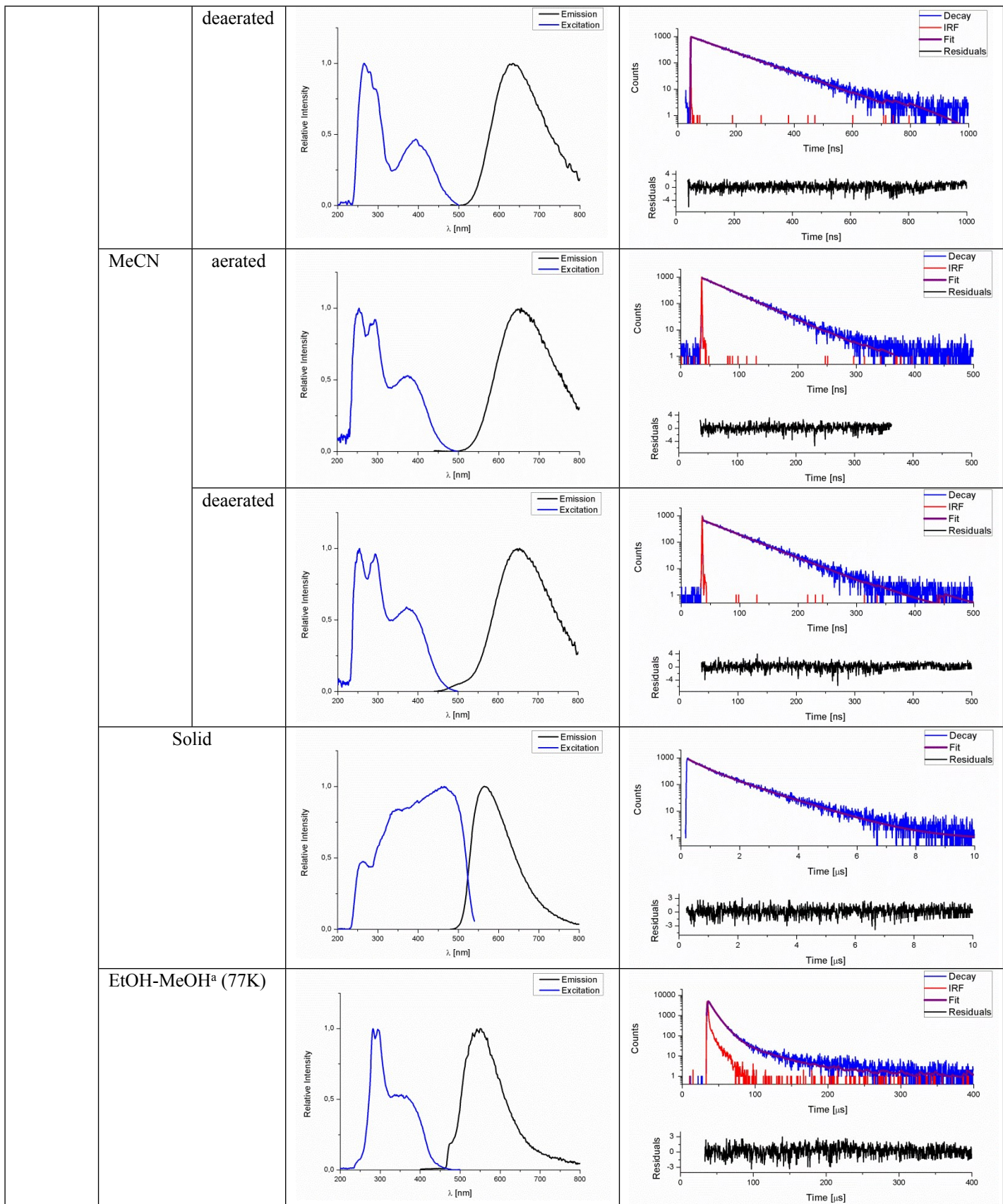
Figure S2. Excitation and emission spectra together with PL lifetime curves for 1-5.











^a(4:1 v/v);

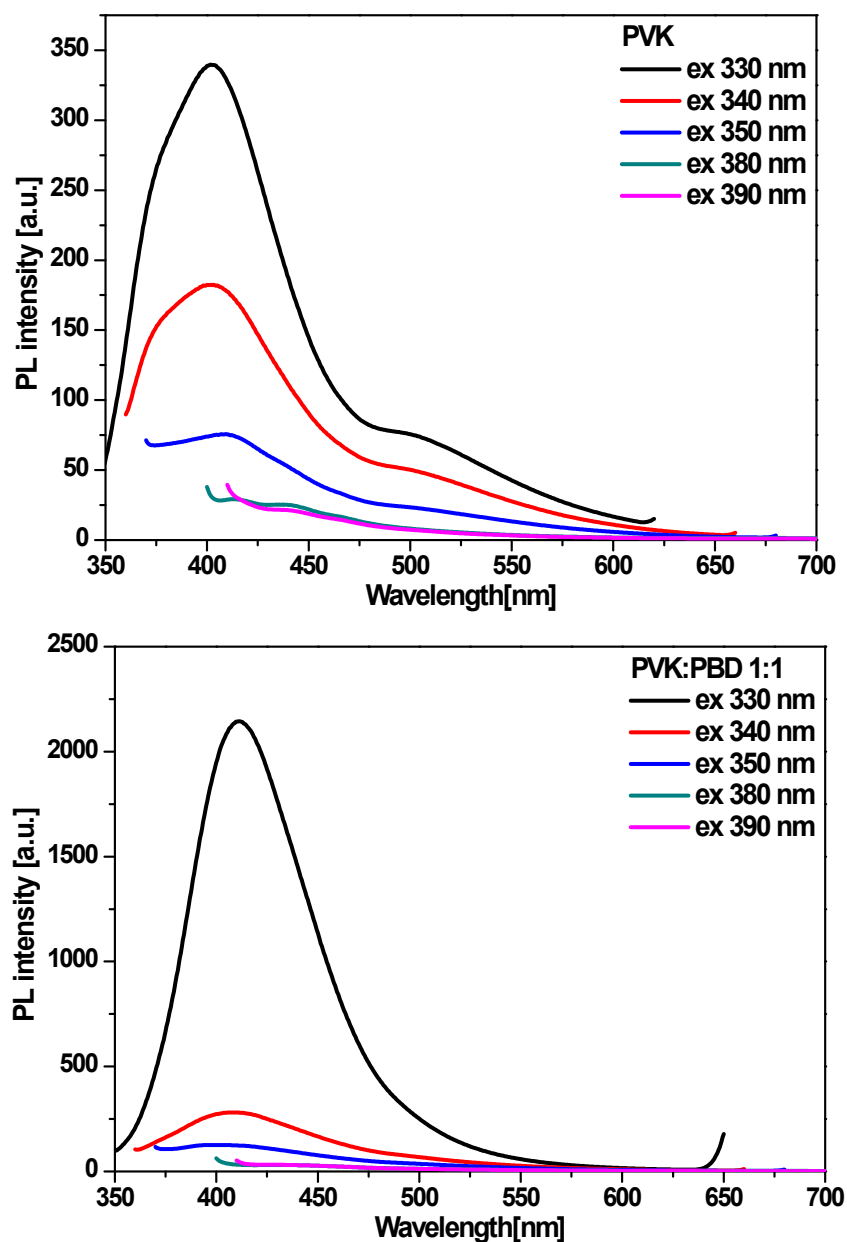


Figure S3. Emission spectra of PVK and PVK:PBD 1:1 films on glass.

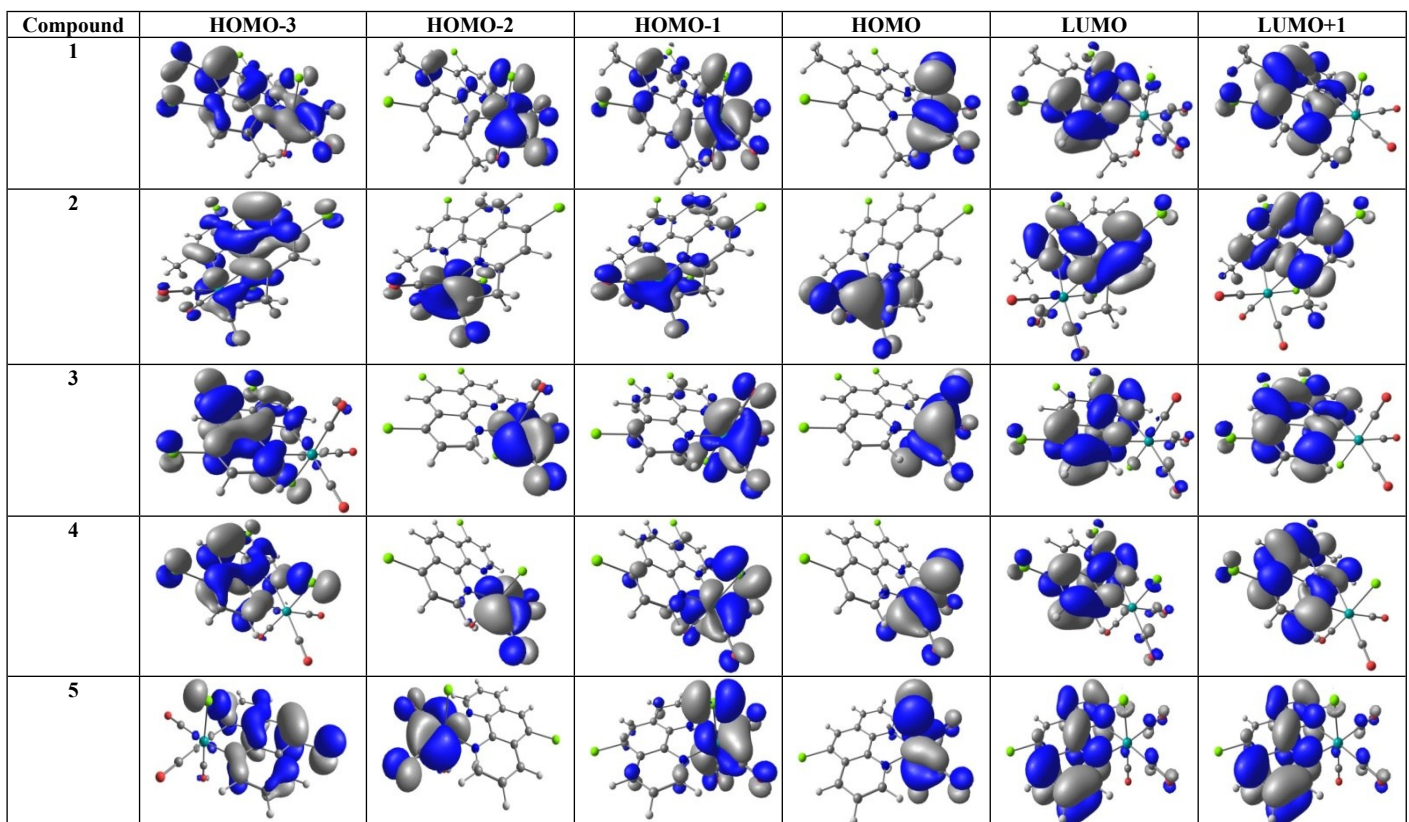


Figure S4. Frontier molecular orbitals of **1–5** computed at the DFT/B3LYP/DEF2-TZVPD level.

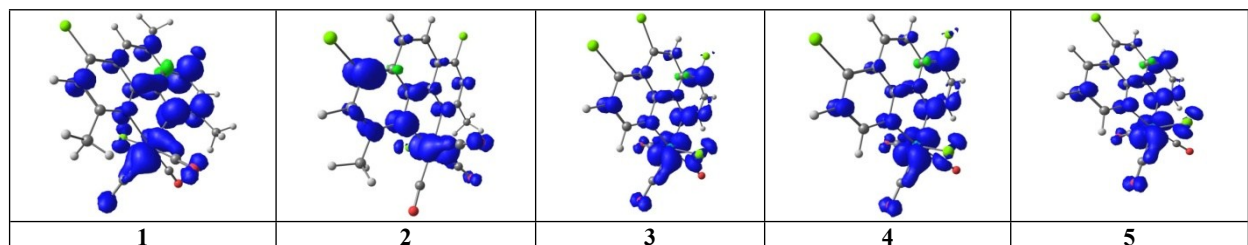


Figure S5. Isodensity surface electron spin density for compounds **1–5** at its T_1 state geometry calculated at DFT/UB3LYP/def2-TZVPD level of theory associated with the PCM model in CH_3CN as a solvent. Blue and green colors show regions of positive and negative spin density values, respectively.

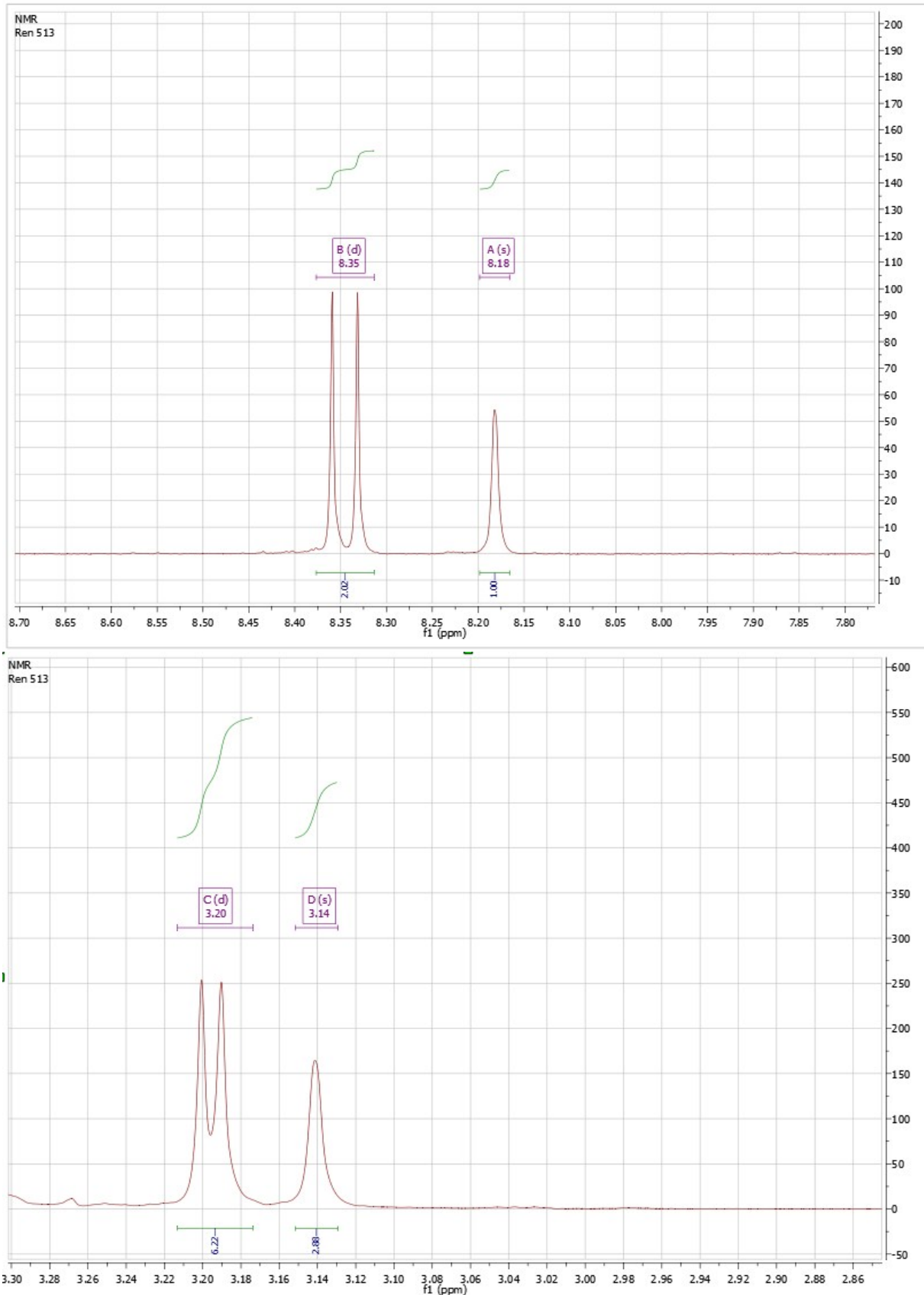


Figure S6. ^1H NMR spectrum of **1**

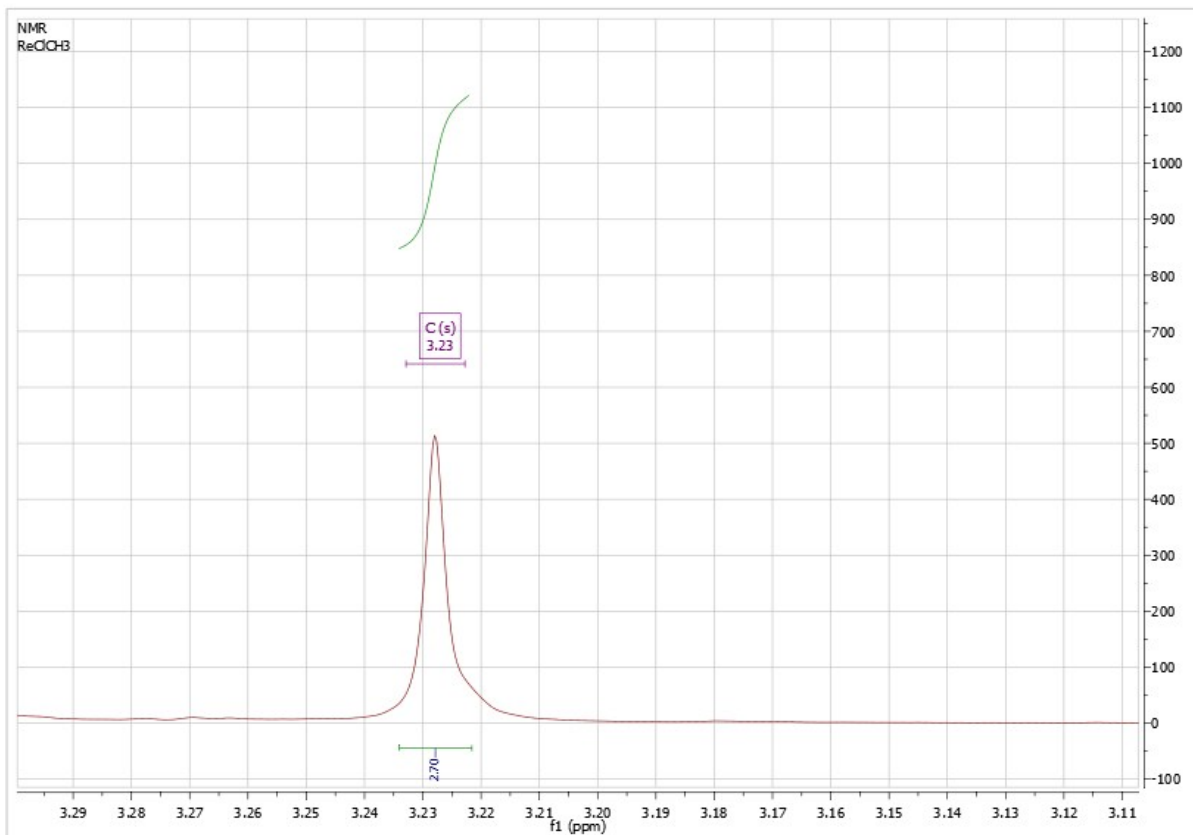
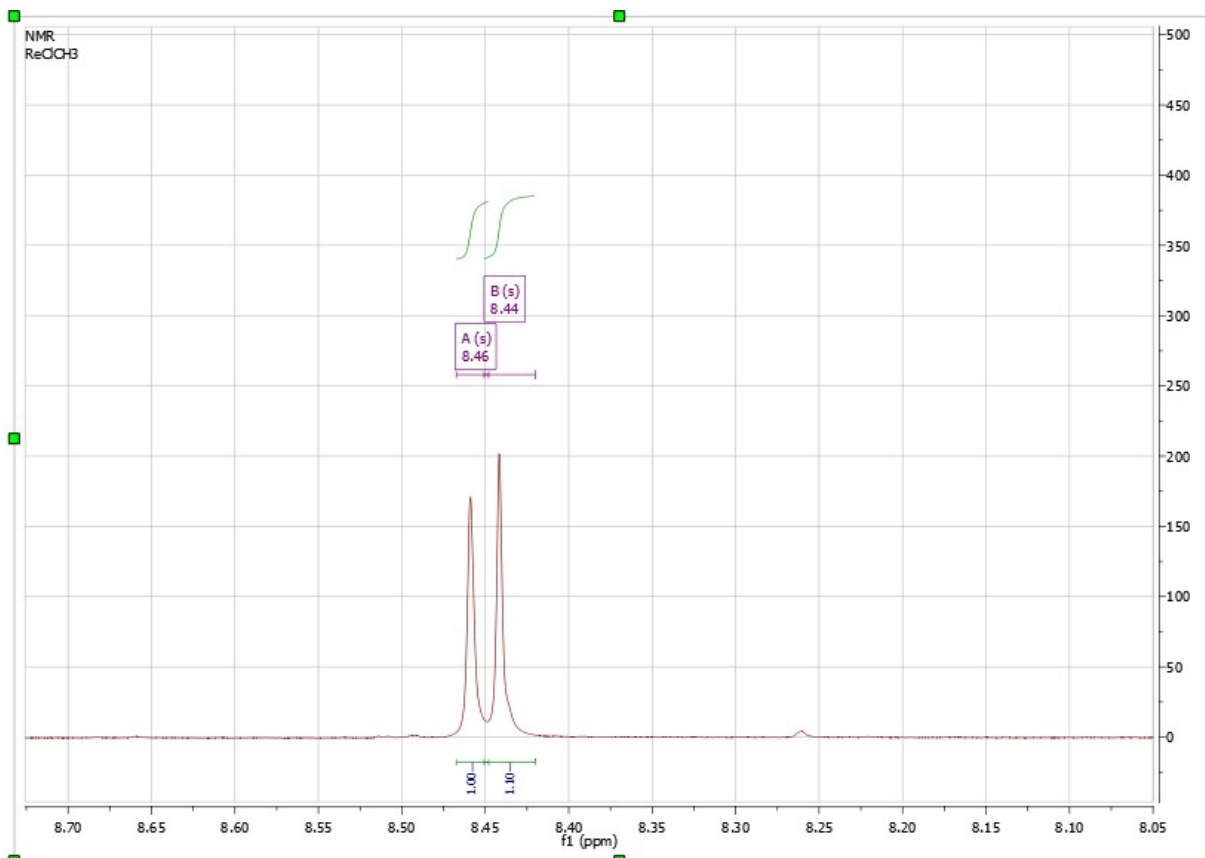


Figure S7. ^1H NMR spectrum of **2**

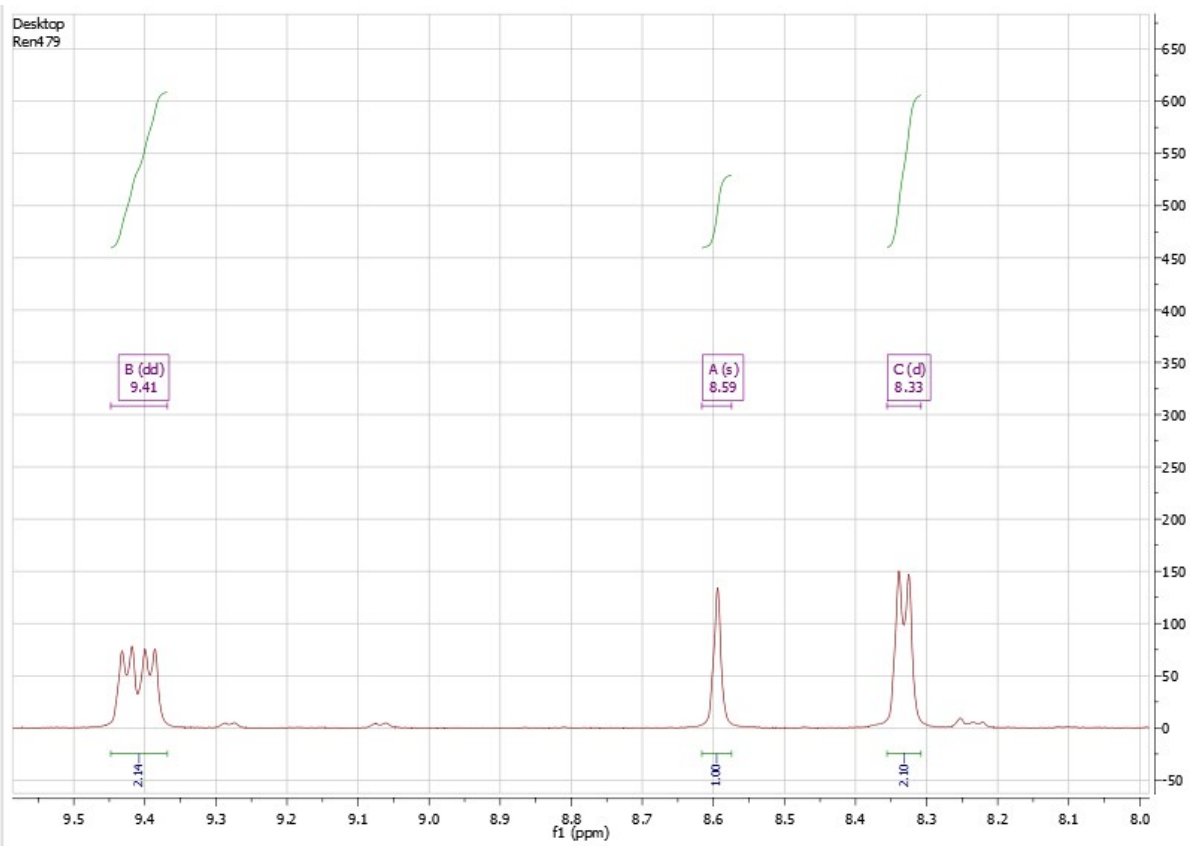


Figure S8. ^1H NMR spectrum of **3**

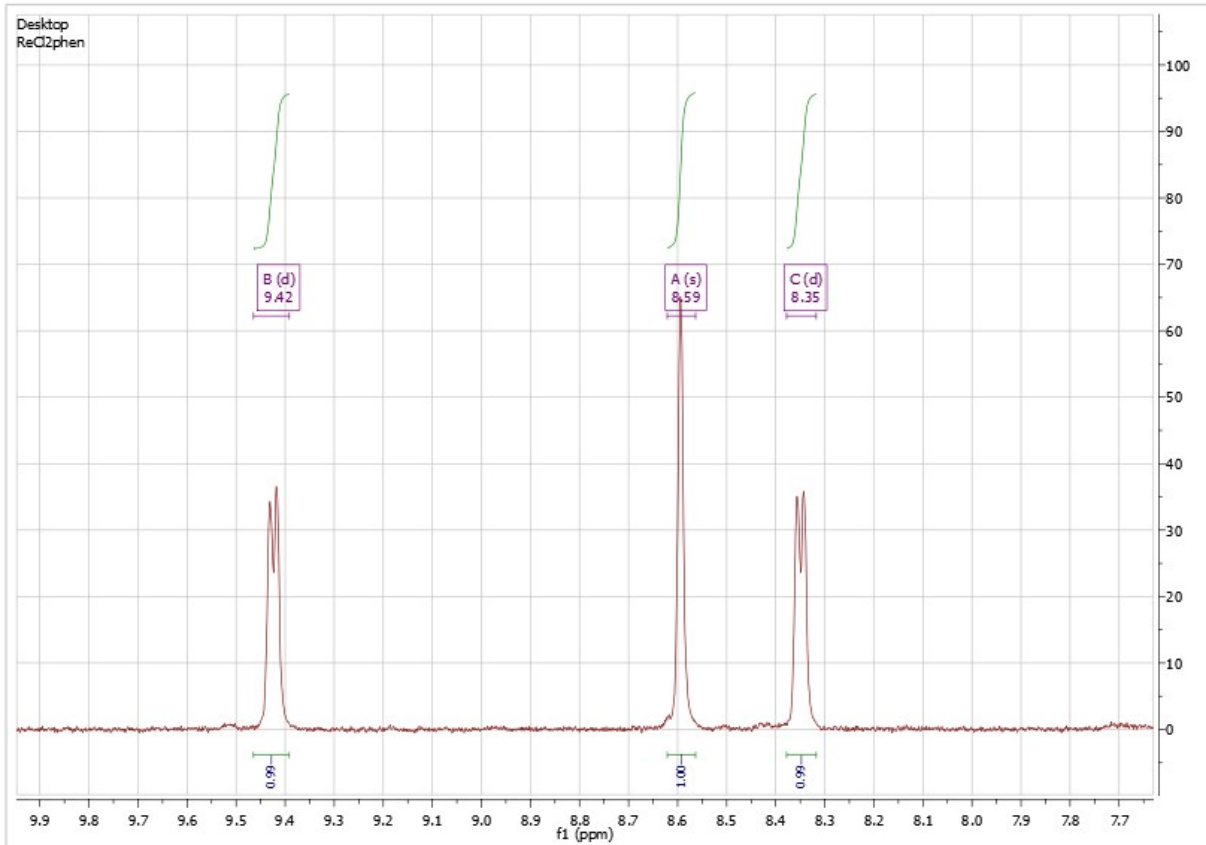


Figure S9. ^1H NMR spectrum of **4**

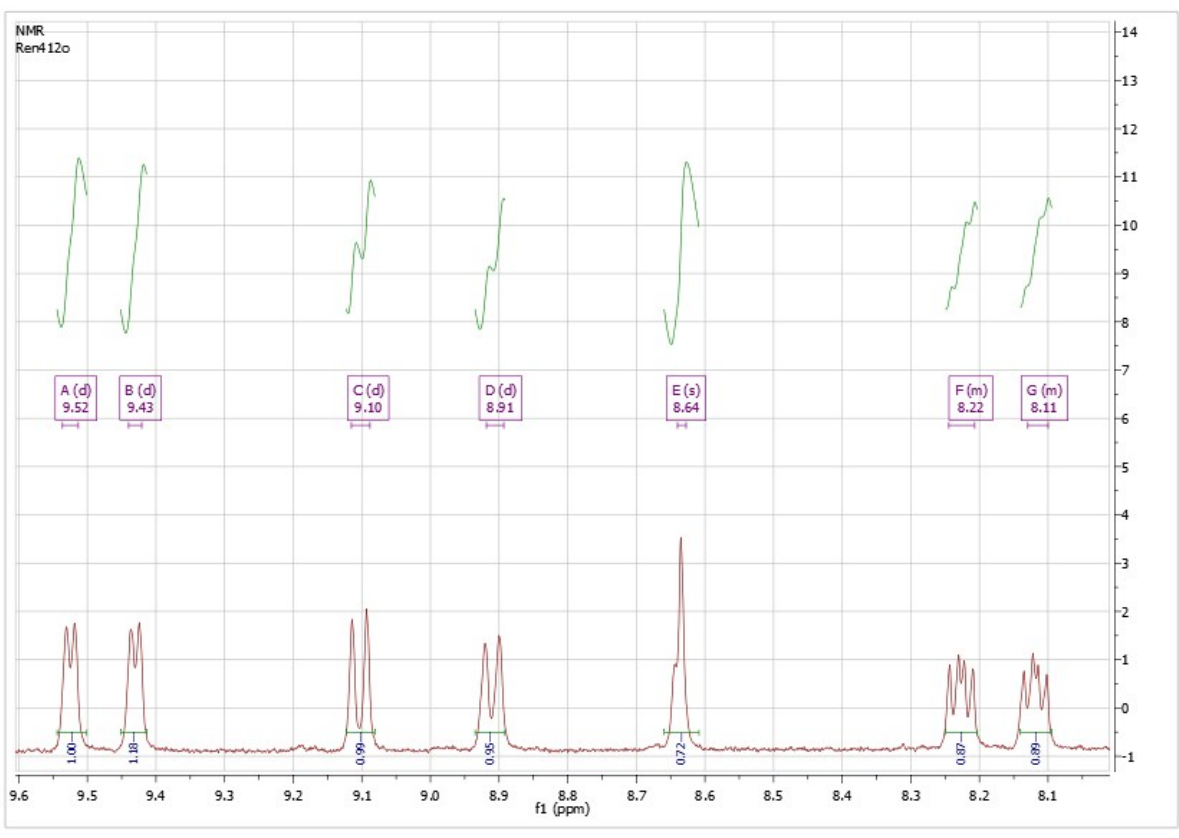


Figure S10. ^1H NMR spectrum of **5**

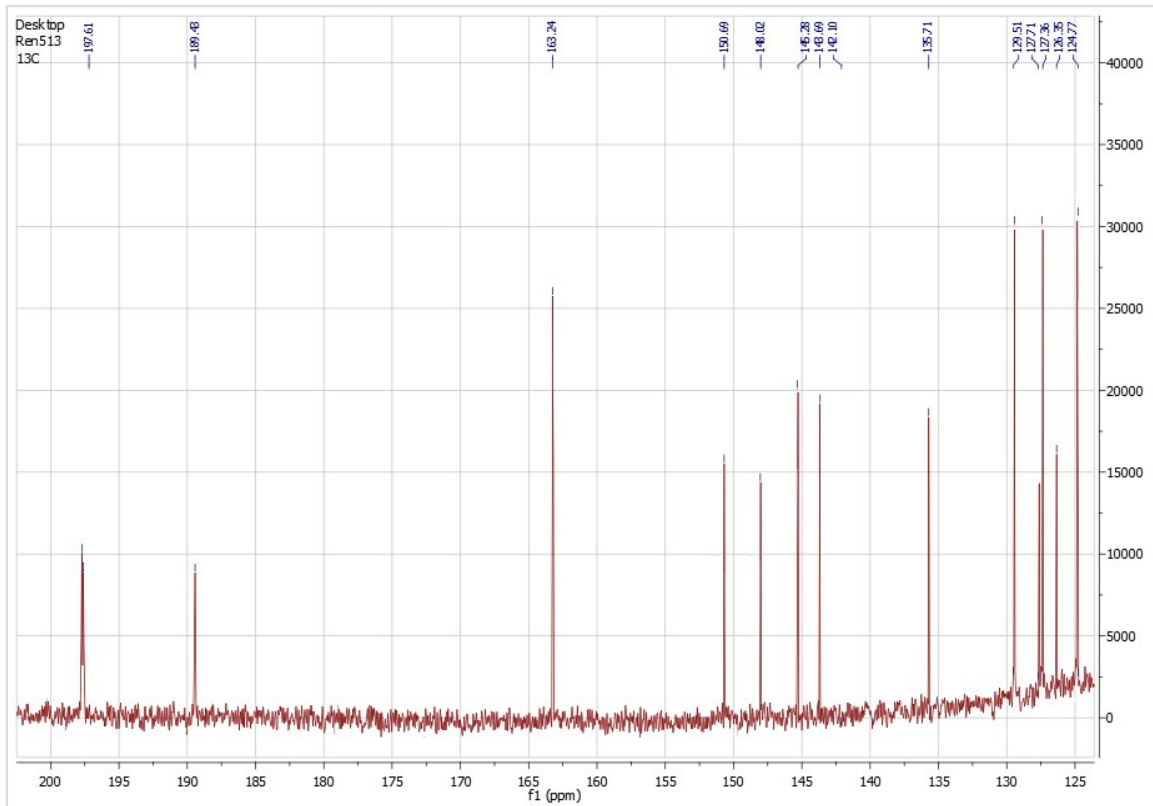


Figure S11. ^{13}C NMR spectrum of **1**

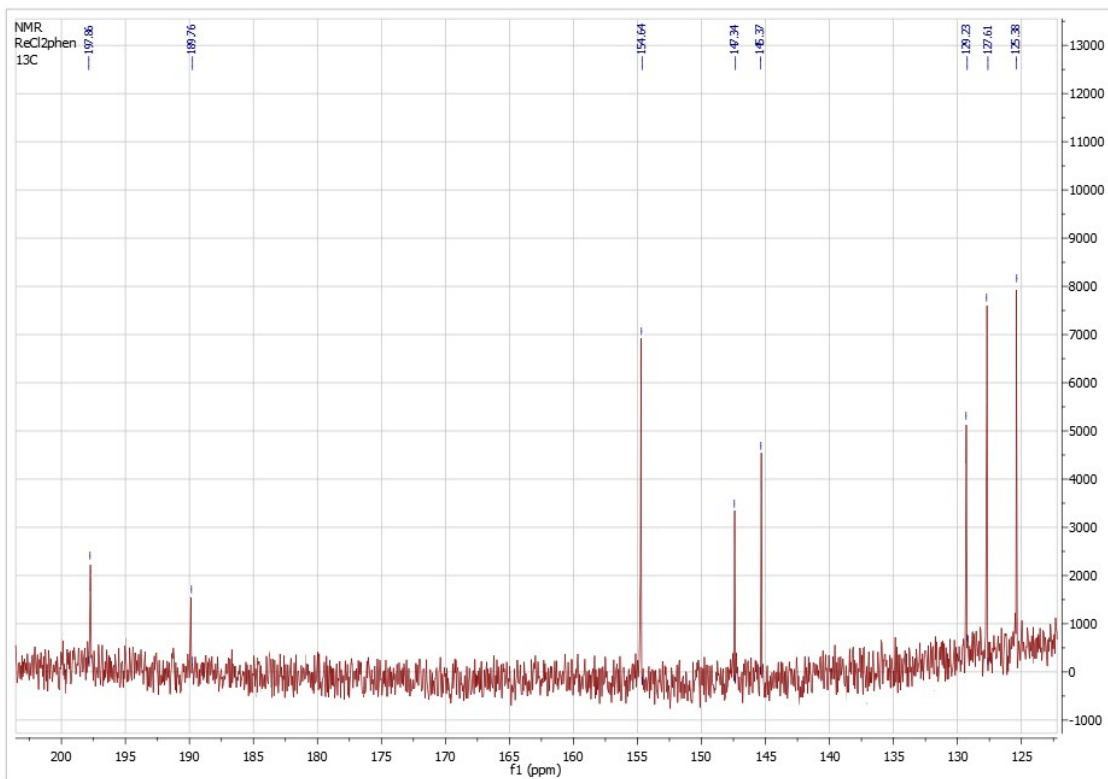


Figure S12. ¹³C NMR spectrum of **2**

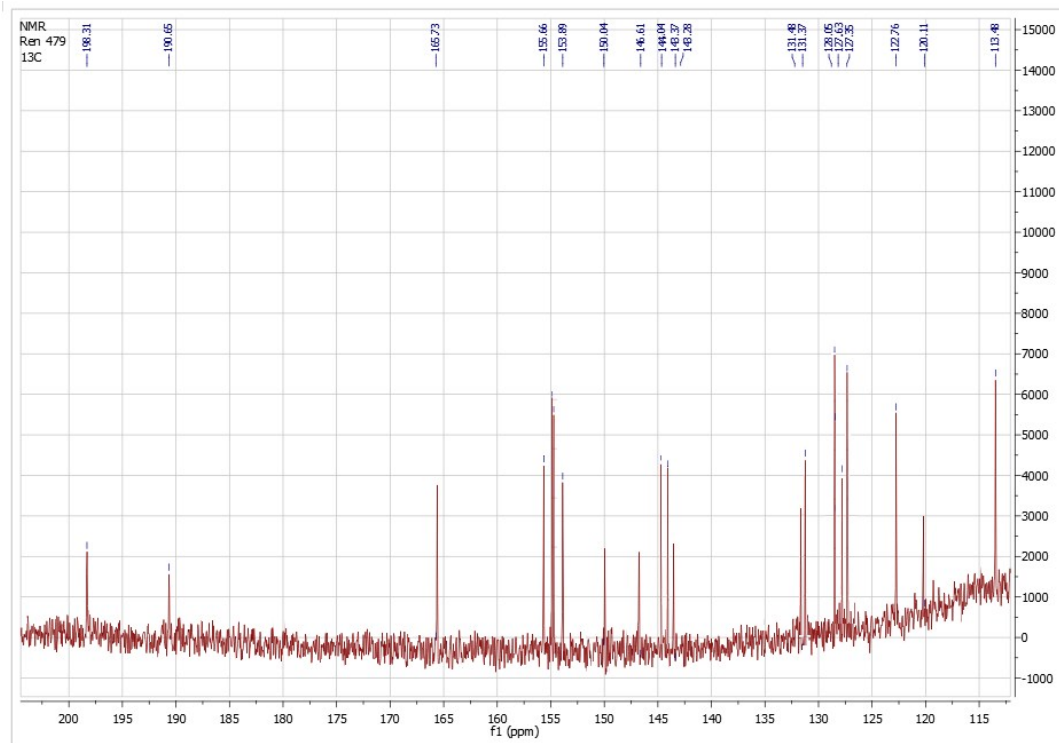


Figure S13. ¹³C NMR spectrum of **3**

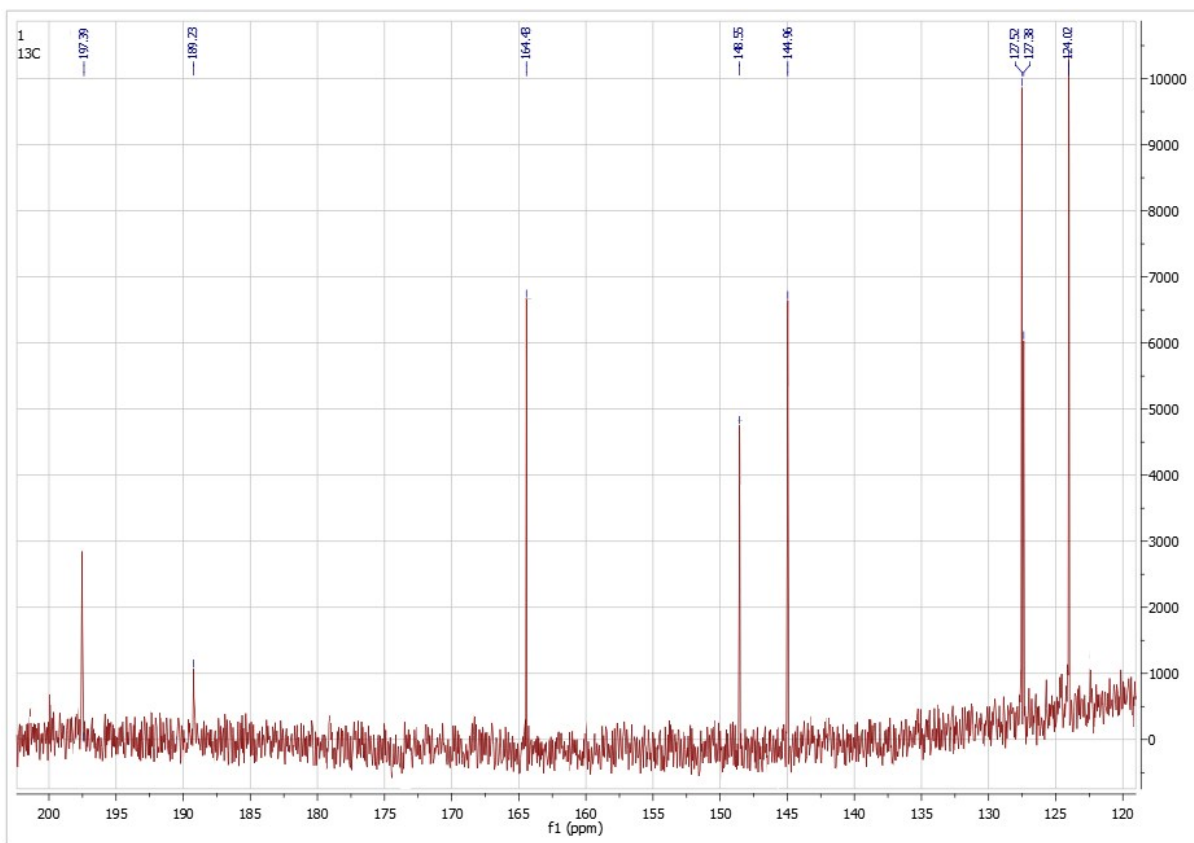


Figure S14. ¹³C NMR spectrum of 4

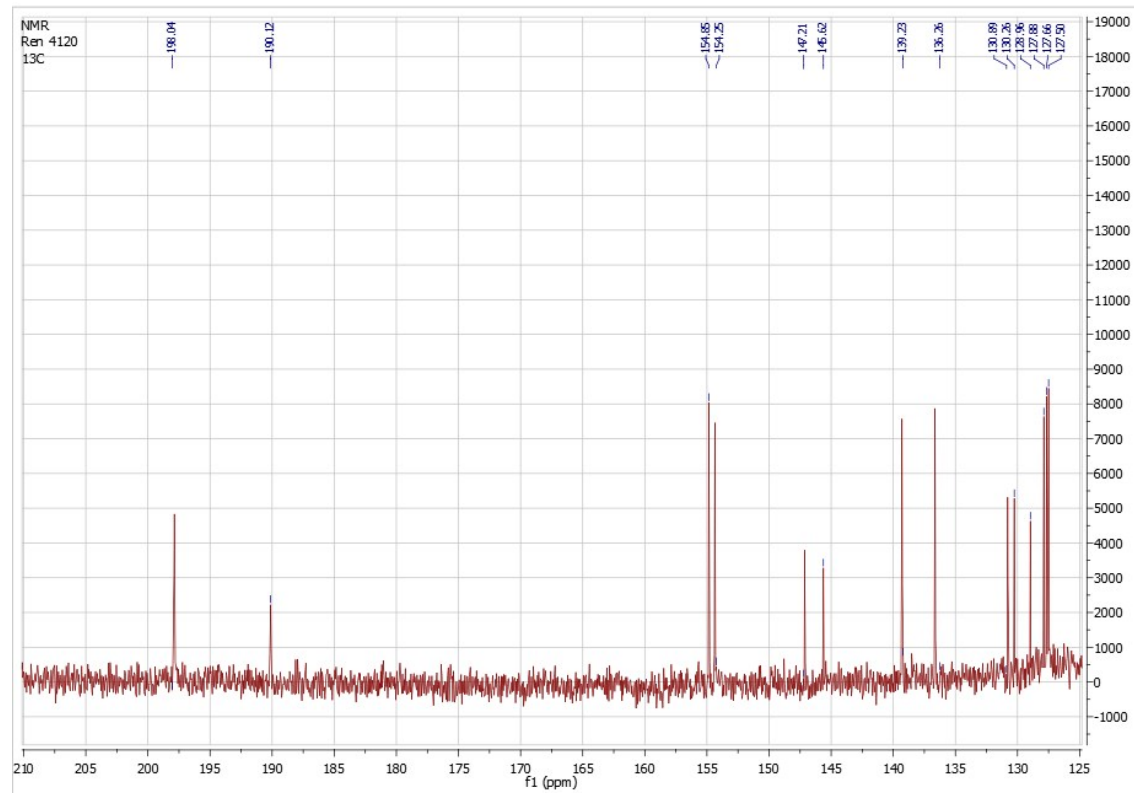
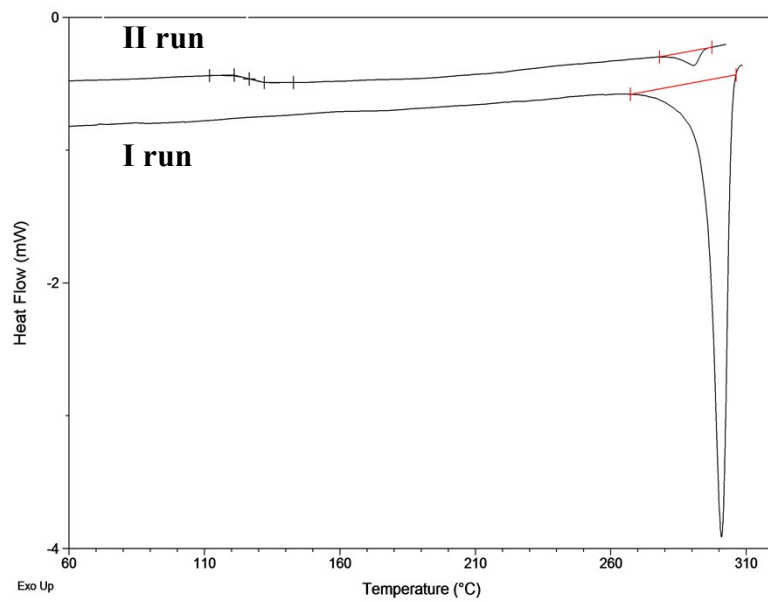
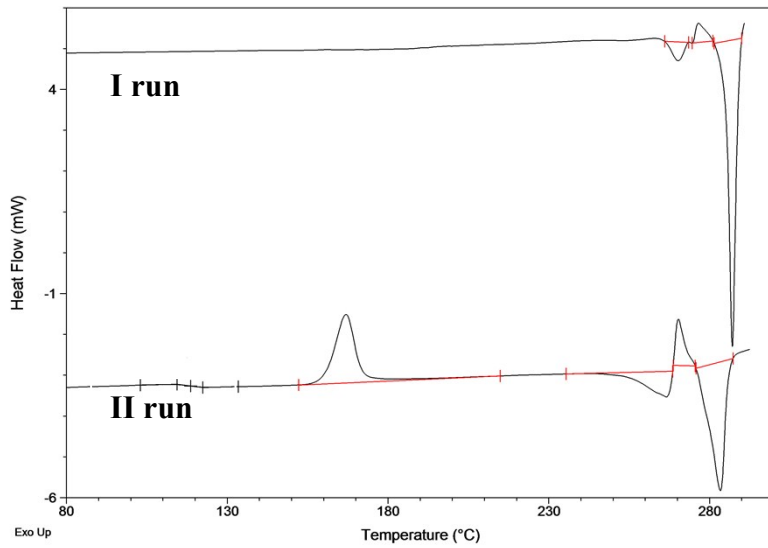


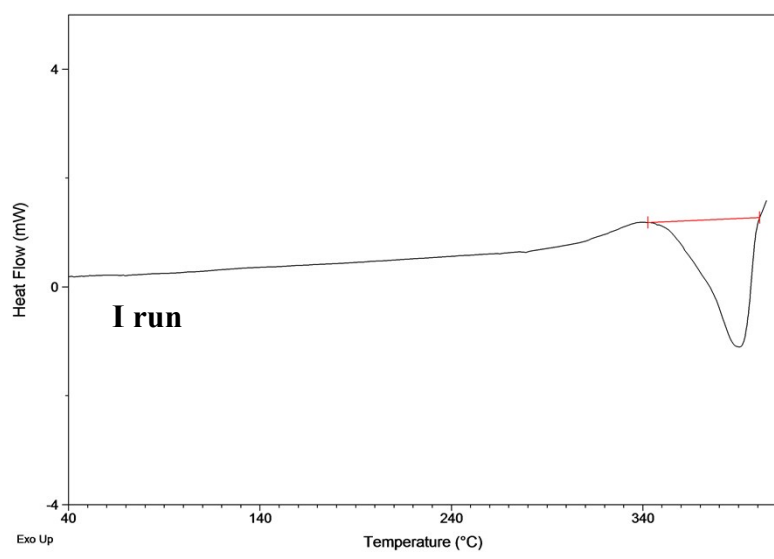
Figure S15. ¹³C NMR spectrum of 5.



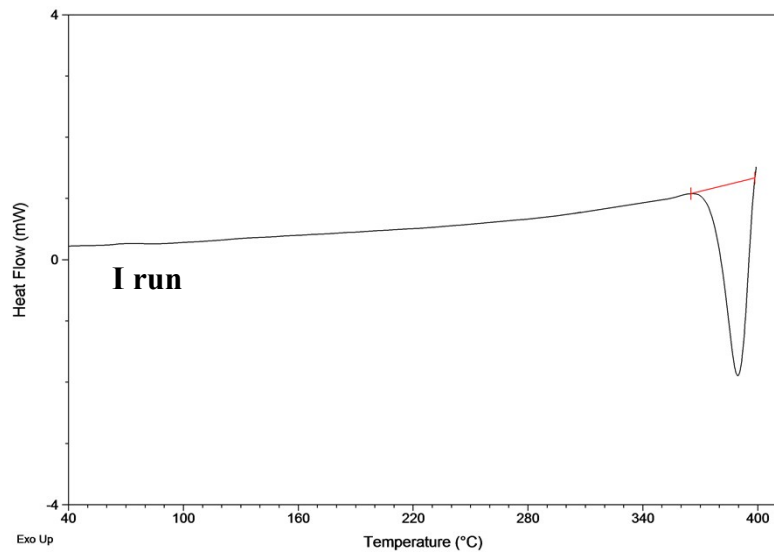
a



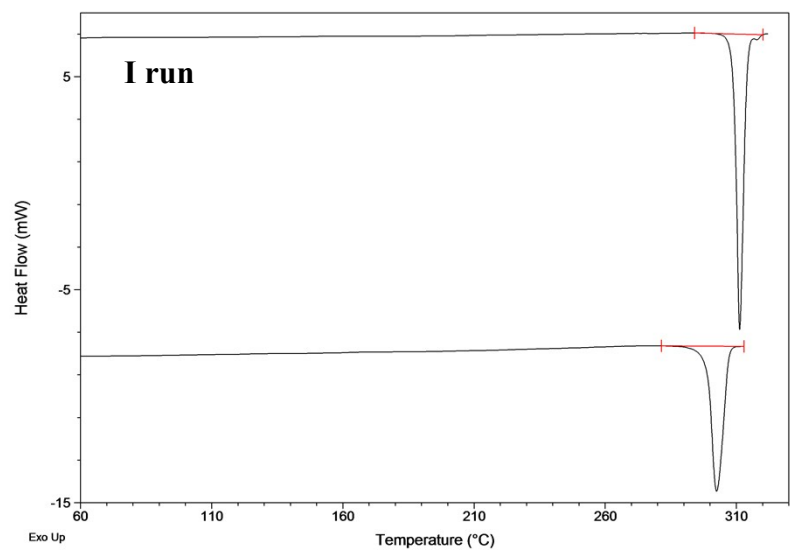
b



c



d



e

Figure S16. DSC thermograms (heating 20 deg/min) of all investigated complexes: (a) compound **1**, (b) **2**, (c) **3**, (d) **4** and (e) **5**.